Faraday cup sizing for electric propulsion ion beam study: Case of a field-emission-electric propulsion thruster

V. Hugonnaud, Stéphane Mazouffre, D. Krejci

Faraday cup sizing for electric propulsion ion beam study: Case of a Field-Emission Electric Propulsion thruster

V.Hugonnaud,[1,2,a] S.Mazouffre,[2,b] and D.Krejci[1,c]
[1)]*Enpulsion, Viktor kaplan straße 2700, Wiener Neustadt, Austria*
[2)]*CNRS-ICARE, 3 Avenue de la Recherche Scientifique, 45100 Orléans, France*

(Dated: 30 July 2021)

This contribution provides information about the sizing and standardization of a Faraday cup (FC) used as a plasma diagnostic. This instrument is used to accurately map the ion beam profile produced by an electric propulsion (EP) device. A Faraday cup is a cylindrical probe which uses an electrode, termed collector, to measure a current. Several studies have shown the relevance of adding an extra electrode, called collimator, to define the collection area and to minimize interactions with the ambient plasma. Both electrodes are encapsulated into an isolated metallic housing which prevent ambient plasma to disturb measurements. In this case study a field emission electric propulsion (FEEP) thruster is used. FEEP technology uses electrostatic fields to extract liquid metal (indium) ions from a sharp surface and accelerate them to high velocities, providing thrust. The FEEP model used in this study is the *ENPULSION NANO* thruster from the Austrian company Enpulsion. We present results focusing on the sizing of a Faraday cup in terms of cup length, aperture diameter, collection solid angle as well as on material exposure to the ion beam. For far-field ion beam study of a FEEP indium based electric thruster our study outcomes show that a Faraday cup optimum sizing is a 50 mm long collector cup and a 7 mm wide inlet aperture. Moreover, shielding the repeller/collimator from direct exposure to the ion beam seems to greatly minimize perturbation during ion current acquisition. Lastly, to only measure the ion current a negative potential should be applied to the collector and repeller where the latter is the more negative. This study contributes to the effort on diagnostics standardization for EP device characterization. The goal is to enable repetitive and reliable determination of thruster parameters and performances.

I. INTRODUCTION

The new space stakeholders ask for more efficient and cost-effective propulsion devices which enable precise and reliable orbital manoeuvres such as orbit modification, station keeping, drag compensation or accurate pointing[1–3]. The last decades showed an interest from the satellite industry into spacecraft cluster and mega-constellations of small communication satellite platforms[4,5]. These platforms are lighter and have a better manoeuvrability than before[6]. The new technical requirements are beyond the scope of passive attitude control and classical propulsion. Numerous electric propulsion (EP) devices[7–10] were developed over the last several decades[11]. An EP device uses electric power to deliver thrust from μN to N with a high exhaust velocity. In this way, an important amount of propellant required for a given space mission is saved. Whatever the technology, thrust is generated via the production and acceleration of charged particles. The various EP technologies rely on different propellants ionisation processes and particle acceleration mechanisms to provide thrust. Therefore, the beam of the EP device, also called plume, differs in term of properties and characteristics. Plasma diagnostics aim to study and characterize electric thruster plumes (i.e. ion beam). It exists different techniques to characterize a plasma created by an EP device[12–24]. They differ from each other in terms of accuracy, implementation, use, data collection and cost. Electrostatic probes are a reasonable trade-off between all these parameters, therefore they are often used. Such diagnostic can extract electron or ion temperature, density, velocity, energy, flux and current from a thruster plume. Many types of electrostatic probes do exist. Their architecture can be elementary such as Langmuir probes[15], simple and guarded planar Faraday probes[22,23]. More complicated designs can be found with additional electrodes like in the case of Faraday cups (FC)[21,25–28] which improve reliability and accuracy. Some are used to filter ion energies and/or velocities like in the case of retarding potential analysers (RPA)[12,29,30], magnetically filtered Faraday probes[31] and E×B probes[18,32]. A FC provides information about the ion current density within the thruster plume. It works by mean of voltage bias applied to an electrode[13,33,34], called collector, to attract ions and repel electrons. Studies[22,23,35] have shown the benefit to use an additional electrode, called collimator, placed at the front of the probe. It defines the collection area and reduces plasma perturbations seen by the collector. Processing the ion current measured by a FC can lead to the determination of key parameters to map the thruster performances such as beam divergence, thrust, current utilization or propellant efficiency. Little studies[35,36] were performed to optimize and standardize Faraday cups so they can be reliable no matter the ion beam nature, hence allowing accurate comparison between different EP devices.

This work deals with the reliability of a Faraday cup compatible with low current densities ($\mu A/cm^2$) and high energy ion beams (up to 10 keV). For this purpose a laboratory version of the *ENPULSION NANO* thruster based on the physics of field-emission-electric propulsion (FEEP) devices is studied. Its ion beam is used to test different Faraday cup lengths, collection areas and front materials. To minimize particle deposition and increase the probe lifetime, an alternative to the col-

[a)]Author to whom correspondence should be addressed:valentin.hugonnaud@enpulsion.com
[b)]stephane.mazouffre@cnrs-orleans.fr
[c)]david.krejci@enpulsion.com

limator electrode is studied. Finally the FC electric field lines were modified to suppress secondary electron, hence avoiding artificial current rise.

II. EXPERIMENTAL APPARATUS

A. Test bench, mechanical interface and instrument

All experiments have been realized inside a cylindrical stainless-steel vessel of 0.91 m in diameter and 1.75 m in length located at the aerospace engineering's department laboratory of Wiener Neustadt University of Applied Sciences (FH Wiener Neustadt). The chamber is equipped with a primary pump having a 70 m^3/h pumping capacity which evacuates a 2200 l/s in N_2 turbo-molecular pump. Without gas injection the residual pressure in the tank goes down to 10^{-7} mbar. During operation of the FEEP thruster the pressure level is typically 4×10^{-6} mbar. Since the chamber is meant to host FEEP thrusters, additional care must be taken regarding materials inside the chamber. Therefore, a 1.32 m long cylindrical aluminium shield is installed inside the chamber to minimize the back flow of indium atoms during operations. It reduces the nominal diameter of the chamber down to 0.67 m. At the back of the chamber deflectors (see figure 1), with sawtooth shape, are installed to minimize the probability to have ions being directly back sputtered toward the thruster in operation.

The holding structure lies on an aluminium plate that is electrically connected to the inner cylindrical shield. The two parts are grounded. The FEEP thruster is mounted onto a 3D printed aluminium plate with heat pipes in order to efficiently control the thruster temperature during operation. The plate is connected to a recirculating cooler (JULABO chiller) to keep the temperature interface down to 15C. The chamber frame is connected to ground. The latter is the reference for the entire experiment.

The FC is installed on an aluminum rotating arm. The structure allows automatic alignment of the probe with the thruster equatorial plane. The Faraday cup holder is mounted on a URS1000BCC motorized rotation stage from Newport controlled from the atmospheric side. The thruster centreline is referred to as the 0 angular position. The pivot point of the rotating structure is aligned with the thruster exit plane. The system enables a scan from -90 to +90 on the horizontal plane that includes the thruster axis. The alignment of the system is done thanks to a laser cross (*TOOLCRAFT CL12*). The distance R between the FC aperture and the thruster exit plane is 26.1 cm. R is in excess of 15 emitter crown diameters. Therefore, the point source hypothesis is valid[28,37,38]. The entire mechanical structured is grounded. The whole experimental set-up is displayed in figure 1.

A calibrated Keithley 2050 sourcemeter is used to measure the ion current collected by the FC collector electrode. The device can be operated from 20 mV to 200 V in voltage source and measures 10 nA to 1 A with 0.012% basic measure accuracy. Additional low voltage power supply units from RND (RND 320-KA3005D 15 W) are used. The power supply can deliver up to ±30 V and 5 A. For direct current measurement on the collimator a Keithley 2410 is coupled to the previously mentioned sourcemeter. The Keithley 2410 device offers a broad range of currents [1 A – 10 pA] and voltages [±1100 V - ±1 V] with a high degree of stability and accuracy.

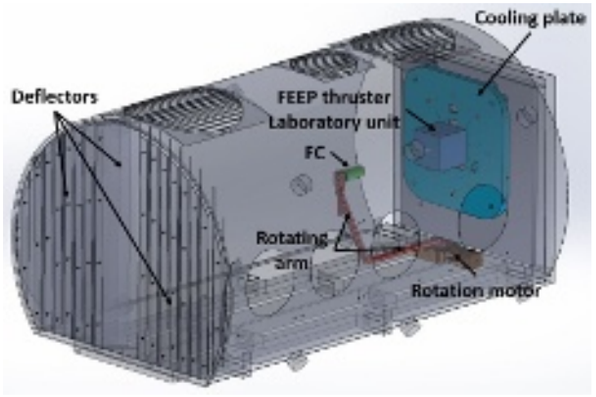

FIG. 1. 3-D model of the experimental apparatus.

A home-made program is used to synchronize all devices to enable accurate control, to record and to save measured data. Note that all current density profiles scan the ion beam from -90 to 90 with step size of 2. The current is averaged from 10 consecutive measurements acquired over 15 seconds at each angular position.

B. *ENPULSION NANO* laboratory unit

The *ENPULSION NANO* is produced by the Austrian company *Enpulsion GmbH*. It is built from the heritage over 20 years of development done at *FOTEC GmbH*[30,39–42]. The thruster is a high specific impulse, liquid indium, field emission electric propulsion (FEEP) system. It enables precise orbit and attitude manoeuvres[43–45]. It has a $10 \times 10 \times 10$ cm envelope and is designed to be easily implemented into satellite structure. It is a 40 W-class thruster suited for formation flight and constellations of small satellites. At time of writing the thruster has achieved significant space heritage with over 65 units in space. Thrust generation is here generated based on FEEP physics[46–48], see figure 2. A strong electrostatic field (10^9 V/m) is applied at the tip of a porous, sharp and wetted structure[49,50]. There, the surface is deformed and the fluid will turned into a cone-like structure, a Taylor cone[51,52]. This configuration emits ionized particles from the tip of the wetted structure[53]. The resulting ion beam is assumed to be composed of ions with some neutrals and thermal electrons (see figure 2). Ions are considered singly-charged. To provide E fields exceeding the emission threshold, called onset voltage, a counter electrode termed extractor (V_{ex}) is used. It aids in both ionization and acceleration process. It enables to reach potentials difference exceeding 10 kV. The core of the *ENPULSION NANO* is a passively fed, porous ion emitter consisting of 28 sharp needle tips, also called injectors (left side in figure 3). The extractor is placed around the crown

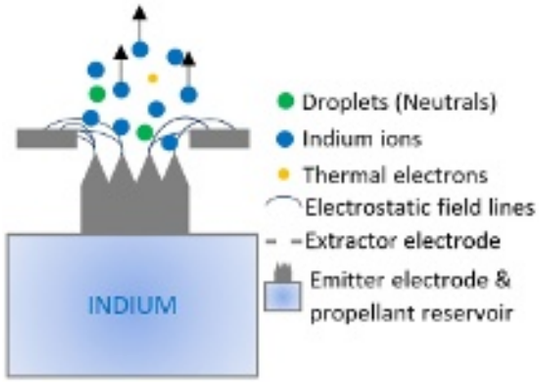

FIG. 2. FEEP thruster working principle.

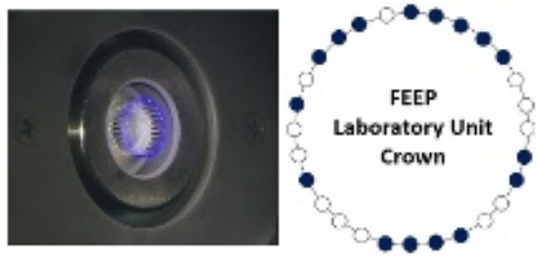

FIG. 3. The flight unit ENPULSION NANO (left) and the indium injectors distribution of the laboratory version (right) used in operation

.

of needles to obtain homogeneous fields. The thruster operates with indium as propellant when the molten metal is in its liquid state. The thruster is fully integrated with a digitally controlled power processing unit (PPU)[45]. It allows accurate control and measurement of the emission voltage (V_{em}) and current (I_{em}). The *ENPULSION NANO* is delivered with two cathodes to neutralize the ion beam during operation.

Results described in this work rely on measurements and analysis of the ion beam produced by a laboratory version of this thruster. Note that the thruster holding structure is grounded to the vacuum chamber wall and to ease the acquisition of the ion signal, direct neutralisation of the low current density ion beam produced by the crown of the thruster is not necessary. The right part of figure 3 shows the crown injectors distribution of the thruster lab version in operation during the campaign. This unit has a firing capacity of 16 well distributed injectors. The reduced amount of firing emitter tips is due to the production process used for this laboratory unit[54]. The PPU can read the firing parameters such as I_{em} and V_{em} with 1% of uncertainty enabling high stability and accuracy during measurements.

Table I gives the two thruster operation points used here. One is meant to assess the impact of the ion energy upon the current collected by the Faraday cup. Therefore, the thruster is kept at 2 mA of current emission (I_{em}) while different emission voltages (V_{em}) are applied. The second point allows the examination of the influence of the current densities on the FC. There, V_{em} is fixed at 8 kV while I_{em} goes from 1 to 3 mA.

TABLE I. Operation points fired during the test campaign. Different thruster mode are assessed. Mode 1 corresponds to constant I_{em} at 2 mA while mode 2 refer to when V_{em} is fixed at 8 kV

I_{em} (mA)	V_{em} (V)	Mode
2	5000	1
2	6000	1
2	7000	1
2	8000	1
2	9000	1
1	8000	2
3	8000	2

TABLE II. Ignition and impedance characterization procedure of the thruster before and after each test.

Step	**Action**	**Duration**
#	#	min
1	Propellant heating and thermal equilibrium	45
2	Slow thruster ignition	20
3	Prior to test impedance characterization	10
4	Setting the operation point	5
5	Measurements	5 to 45
	Repeat steps 4 and 5 if needed	
6	Post test impedance characterization	10
7	Propellant cool down and vacuum chamber opening	-

To enable stable thruster operation the same procedure is followed for each experiments, see table II. The first steps is to bring the thruster to operational mode by heating up the propellant and reaching injectors stability. Then, prior to operate the Faraday cup, a thruster impedance characterization is realized. There, the potential of the counter electrode (i.e. extractor) is fixed to -4 *kV*, -6 *kV* and -8 *kV* while a current sweep is done. It allows to compute the electrical impedance Z of the thruster[45]. This parameter provides information on the performance stability of the thruster between each set of test. Step 4 and 5 correspond to ion current acquisition with the Faraday cup. Once measurements are over, an additional impedance characterization, similar to step 3, is done.

C. Faraday cup architectures

Thruster properties such as thrust level, specific impulse (Isp), divergence angle, propellant and current utilization (α and η_b) are of interest to build a performance map. They are determined by the flux of ions which form the electric thruster plume. Numerical plume modelling[55–57] can be constantly improved thanks to more accurate and reliable experimental measurements of the ion flux produced by an EP device.
The ion current density can be measured via an electrostatic probe. In general, Langmuir and planar probes are used as they are affordable and easy to build. However, both are extremely sensitive to ambient plasma and sheath effects. It makes data post-processing laborious[14,22] and mathematical models[13,17,58] are necessary to counteract these effects and

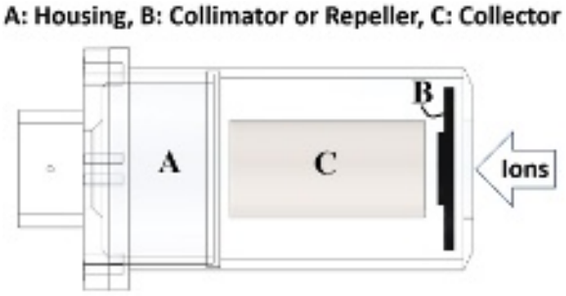

FIG. 4. Main parts of a Faraday cup

current density uncertainty is large. A Faraday cup (FC) is more elaborated than the previously mentioned probes but its physics and architecture remain simple. An FC is an isolated conductive open cylinder, termed cup, dedicated to the detection of charged particle. When a Faraday cup acts as an ion collector, the ion current in the probe direction can be accurately measured. Thanks to the FC closed geometry, edge effects are negligible.

Figure 4 displays the main components of a FC. The pod or housing (A) is grounded and shields electrodes from ambient plasma. The FC here is insulated with PEEK from any conductive part of the probe. Inside, the collimator electrode (B) is used to define the ion flux entering the diagnostic. The latter needs to have the smallest orifice of the system. It screens thermal electrons and acts as a filter for ion velocity vector. In this manner, it avoids saturation of the measurement chain when the FC is placed in the centre of the ion beam. It is the most exposed part to the ion beam. Then, it needs to support high level of stress such as heating, pulverization, deposition. The collimator sits right behind the housing front. To minimize confusion between collector and collimator electrodes, the latter will be termed repeller in the next sections.

Finally, the collector electrode (C) is used to collects the collimated ion flux[13,33,34]. The collector is subject to heavy ion bombardment and sensitive to subsequent ion induced electron (SE) emission. Based on different studies which aimed at enhancing ion collection and minimize secondary electron emissions[59–63], the collector diameter is fixed to 12 mm and the rear side of the cup is a AlSi7Mg open-cell foam disk (Nr.4) provided by Exxentis[64]. Each pore has a diameter between 0.4 to 1 mm and is connected to others via channels with 0.15 to 0.2 mm diameters. The whole volume porosity is $60 \pm 5\%$. SE are minimized but not suppressed with such collector properties. Therefore, in this work a battery of test is conducted to assess the impact of different probe parameters (cup length, internal FC field lines) on secondary electron recollection.

Figure 5 shows the various architectures studied in this work. For the sake of clarity a nomenclature (ID) is used to identify all Faraday cups. Each ID includes four components in the form X.X.X.X.

- The first element represents the length of the cup. It can be 50 mm, 30 mm or 10 mm.
- The second element refers to the material facing the beam. It can be either graphite (G), molybdenum (Mo) or aluminium (Al).
- The third one informs on the inlet aperture diameter d_a. It can be 10, 07, 05, 03 or 01 mm.
- The fourth element gives information on the position of the repeller. If the repeller is exposed to the ion beam and collimates the ion flux, then the letter E is used. On the contrary, when the repeller is placed behind the housing and the housing front aperture d_{pod} is smaller than the collimator aperture diameter d_r, the collimator is considered protected from the ion beam and the letter P is used.

For example, the FC identified as 30.G.07.E refers to a Faraday cup with a 30 mm long cup where the front part of the probe is in graphite, the opening diameter is 7 mm and the collimator is in the configuration where it is exposed to the plasma. A FC called 50.Al.05.P has a cup of 50 mm, its front material is aluminium, its aperture is 5 mm and the collimator is protected from the ion beam.

III. DATA PROCESSING

A. Beam Parameters

1. *Ion current I_i*

The current density distribution j_i over a hemisphere permits to compute beam parameters such as ion current ($I_{i_{int}}$), thrust (T), thrust vector deviation, divergence angle (θ_{div}), thrust loss factor (F) and current utilization (η_b). The ion current is determined using the hypothesis of cylindrical symmetry of the ion beam around the thruster axis. The formula reads:

$$I_{i_{int}} = \pi R^2 \left[\int_0^{\frac{\pi}{2}} j_i(\theta) \sin(\theta) d\theta + \int_0^{\frac{-\pi}{2}} j_i(\theta') \sin(\theta') d\theta' \right]. \quad (1)$$

This being equivalent to:

$$I_{i_{int}} = \pi R^2 \int_{-\frac{\pi}{2}}^{\frac{\pi}{2}} j_i(\theta) \mid \sin(\theta) \mid d\theta. \quad (2)$$

The mathematical logic behind equations 1 and 2 is demonstrated in previous publication[23,65]. Often the shape of an EP device beam is assumed to be Gaussian. The crown of the *ENPULSION NANO* is composed of 28 single injectors. If the whole crown is firing this assumption might holds. However in our experiment only 16 injectors fire, see figure 3. It makes the hypothesis of a Gaussian shape disputable as exemplified in figure 6. The Gaussian only correctly fits half of the experimental profile. Consequently, here raw j_i distributions are integrated using equation 1. The Simpson's rule is applied for numerical integration.

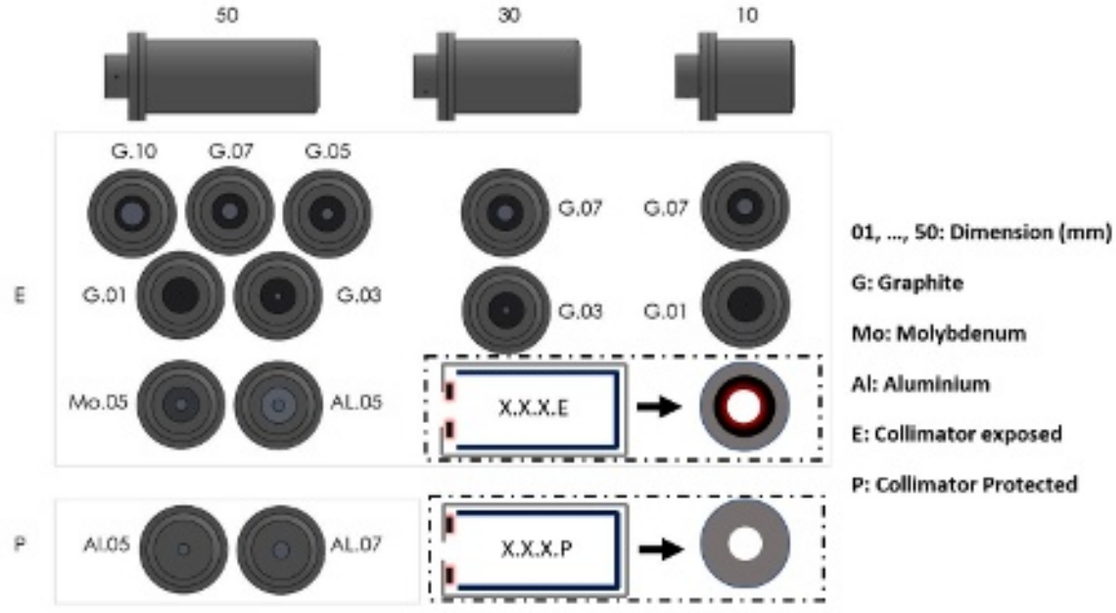

FIG. 5. Nomenclature used in this study to recognize all Faraday cup architectures.

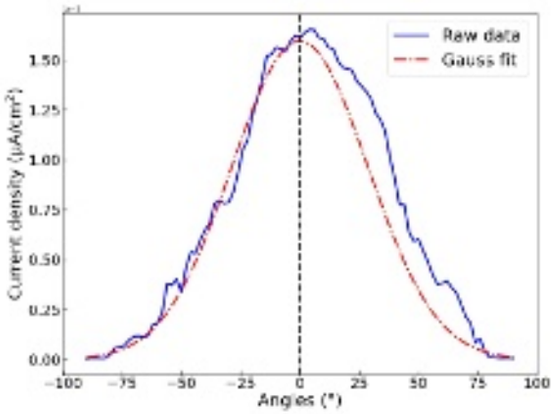

FIG. 6. Gaussian fit compared to raw current density angular distribution. The thruster is operated at 2 mA, 6 kV is applied to the emitter and -8.6 kV to the extractor.

2. *Beam divergence, thrust, thrust loss factor and thrust vector*

The beam divergence refers to the width of the beam. The latter can be estimated using the half-angle θ_{div} computed from $I_{i_{int}}$. It is common to assume that $I_{i_{\theta_{div}}}$, the current corresponding to θ_{div}, is 95% of the measured ion current[22,23,66]. Therefore it reads:

$$I_{i_{\theta_{div}}} = \pi r^2 \int_0^{\theta_{div}} j_i(\theta) \cdot \sin(\theta) \cdot d\theta = 0.95 \cdot I_{i_{int}}. \quad (3)$$

However, an effective plume divergence angle (λ) is often used[36,66] to consider momentum losses associated to plume divergence when one wants to compute thrust. λ accounts for calculation of losses due to the fact that some ions are not travelling parallel to thruster axis. It corresponds to the ratio of the axial ion current and the total ion current $I_{i_{int}}$. λ reads:

$$\lambda = \arccos\left(\frac{I_{axial}}{I_{i_{int}}}\right) \quad (4)$$

$$\lambda_{=} \arccos\left(\frac{\pi R^2 \left[\int_0^{\frac{\pi}{2}} j_i(\theta)\cos(\theta)\sin(\theta)d\theta\right]}{\pi R^2 \left[\int_0^{\frac{\pi}{2}} j_i(\theta)\sin(\theta)d\theta\right]}\right)$$

Equations 3 and 4 show the way $I_{i_{int}}$ is calculated (smoothing, fitting, filtering, interpolation) greatly influences the value of θ_{div} or λ for a given dataset. Consequently, an accurate design of a FC should reduce at maximum data processing and treatment.

The thrust loss factor F is used to correct the thrust[7,45,66,67] for effects of plume divergence, energy spreading or losses. The thrust therefore reads:

$$T = I_{i_{int}} F \sqrt{2 V_{em} \frac{m}{q_e}}. \quad (5)$$

For FEEP thrusters, F can be approximated using cosine factors[67] from the effective beam divergence[66,68]. The equation was experimentally verified by direct thrust measurement[47]. Here, indium ions are considered singly-charged[69]. The emitter potential (V_{em}) is assumed to be equal to the ion energy eV_{em} without energy transfer losses[30,70]. Note that beam deviation for each injectors due to Taylor cone

deformation is not considered in this study. Mühlich et al[57] showed that once the emitter crown is firing with many needles, collective effect takes over single behaviour. Therefore, the thruster plume is considered as a whole and not as the sum of single ion beams. One must consider the F factor as simple tool which gives, nevertheless, a good first estimation of the losses[45].

Additionally, the beam deviation or thrust can be found with 3D ion current measurements. Here the beam deviation can be accurately determined only in the horizontal plane due to our 2D measurements. Each component of the current density angular disposition is weighted to obtain the angular deviation (ζ), in degrees, of the beam from the thruster axis. Finally, the efficiency of the Faraday cup (η_p) is used to evaluate and compare FC designs. In the case of a FEEP thruster, emission current is achieved in direct mode control. Therefore the integrated ion current $I_{i_{int}}$ should ideally be equal to the emitted ion current I_{em} recorded by the power supply. Due to small current oscillation during plume scanning, a value of I_{em} averaged over 800 data points is used to compute η_p. The probe efficiency reads:

$$\eta_p = \frac{I_{i_{int}}}{I_{em}}. \tag{6}$$

For an ideal FC the ratio equals 1. In reality errors only allow to have an integrated ion current close to the emitted current I_{em}, see next section. The parameter η_p is therefore the right figure of merit to optimize a FC architecture.

B. Measurement accuracy

Table III gathers parameters considered to define the total uncertainty on the integrated ion current, probe efficiency η_p. Uncertainty is computed with the following equation

$$u = \frac{\sigma}{\sqrt{n}}, \tag{7}$$

Where σ is a standard deviation and n the number of acquisitions. All uncertainties listed in Table III are obtained using a linear error propagation with 95% confidence level, which reads:

$$u = \sqrt{\sum_{i=1}^{n} u_i^2},\ u_{95\%} = 2u \tag{8}$$

During current density angular distribution measurements (section VI and VII) ten consecutive acquisitions are performed at each probe angular position. The emission current and voltage read by the thruster on-board telemetry is averaged over a 800 samples, it gives an uncertainty of 0.01% that is negligible compared to the telemetry reading accuracy ($\sim$1%). From our budget uncertainty we are able to provide probe efficiencies and SE trapping yield ($\gamma_{L_{SE}}$) with $\pm$3% accuracy (section VI and VII). Moreover, for non-linear parameters like the thrust T (see appendix) a more complex form of error propagation is used:

TABLE III. Parameters considered in the uncertainty budget.

Parameter	Uncertainties
#	%
Probe pointing and positioning (Alignement, distance and rotation)	$\pm$1.15%
Acquisition system (Keithley 2450)	$\pm$0.012%
Telemetry (PPU)	$\pm$1.0%
Probe cleanness	$\pm$0.28%
Pressure (pressure gauge)	$\pm$0.11%
Total	$\pm$1.5%
Total with 95% confidence	$\pm$3%

$$\frac{u(T)}{T} = \sqrt{\left(\frac{u(V_{em})}{2V_{em}}\right)^2 + \left(\frac{u(I_{i_{int}})}{I_{iexp}}\right)^2 + \left(\frac{u(F)}{F}\right)^2}. \tag{9}$$

Note that the main uncertainty involved in thrust computation comes from the thrust loss factor F with a value around $\pm$10%. Therefore $u(F) \gg u(V_{em})$ and $u(I_{i_{int}})$. Consequently, experimental thrust (see appendix) can only be computed within $\pm$10% measurement inaccuracy. Experimental results will also be compared to outcomes of a numerical model used by the thruster telemetry[45]. Krejci et al. were able to show proof to validate a mathematical model as they compared computed thrust against direct thrust measurements conducted at the ESA Propulsion Laboratory (EPL). The measured thrust was calculated with uncertainties between $\pm$6 and $\pm$11% for high and low thrust mode respectively. In our case study, the thruster fires in mode 2 at 1 mA, 2 mA and 3 mA. Therefore, thrust computed with the thruster telemetry mathematical model will have uncertainties of $\pm$11%, $\pm$7.5% and $\pm$6% from the lowest to the highest thrust.

IV. PERTURBATIONS

Introducing an object inside the main beam of an EP device disturbs the plasma. The FC front material withstands important level of stress when bombarded with highly energetic ions. In such conditions any material might experience three phenomena. Figure 7 displays three possible scenarios when a primary ion ("+" - dark blue) reaches the target:

- Ions rebound or reflection ("+" - light blue)
- Atoms (i.e Neutral) sputtering ("N" - green)
- Ion induced electron (SE) emissions ("$-$" - red)

In the case of ion rebound, the reflected particle would not be collected. Nevertheless, if a series of rebound follow the initial impact, then the charged particle may be properly captured. The closed architecture chosen for all FCs presented in this work is designed for minimizing such effects and prevent ion losses. Moreover, the foam material used as collector electrode enhance ion collection thanks to its pores and internal channels.

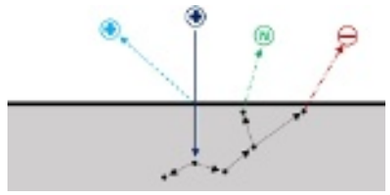

FIG. 7. Ion rebound, atom sputtered and ion induce electron emission due to ion impact into a material surface

Atom sputtering is characterized by its yield. It defines the ratio of emitted atoms per incident ions. It is greatly dependant upon the target material properties and the projectile energy. Most of the ejected particles are neutrals, therefore they will not directly contribute to the measured current. However, if the same neutrals hits the collector due to the Faraday cup close geometry, it will contribute to the process of electron emission from the material surface.

Secondary or ion-induced electrons (SE) are the predominant perturbations during ion current measurements with a FC and more generally with any type of electrostatic probe. Once a primary ion is collected an electron can be ripped off the target surface and ejected. Consequently, the current measured on the collector is artificially increased and reads $I_c = I_{i_{SE}} = I_i + I_{SE}$. With I_i the ion current and I_{SE} the current contribution of ion-induced electrons. It is related to the ion current measured $I_{i_{meas}}$ as $I_{SE} = \gamma_{SE} \times I_{i_{meas}}$. The factor γ_{SE} informs on the amount of secondary electrons emitted by a material; the lower the yield the lower the impact on the measurements. In section VI we experimentally determine the amount of SE escaping the cup according to the length of the latter. Therefore, the coefficient $\gamma_{L_{SE}}$, as opposed to γ_{SE}, does not directly relate to the material properties. It defines the capacity of the cup to trap SE and prevent them to leave the collection system. It reads:

$$\gamma_{L_{SE}} = \frac{I_{i_{SE}} - I_{i_{meas}}}{I_{i_{meas}}}, \tag{10}$$

Figure 8 pictures the way both $I_{i_{SE}}$ and $I_{i_{meas}}$ currents are measured in our experiments. The collector is biased negatively ($V_{collector}$) to always attract ions. A negative potential is applied to the repeller ($V_{repeller}$) as well to shield the collector from thermal ions and electrons. When $V_{collector}$ is more negative than $V_{repeller}$, SE released by the collector escape the collection system as explained by *Case* 1 in figure 8. However, once $V_{collector} > V_{repeller}$ (*Case* 2) SE are redirected to the cup, therefore the measured current will be the true measured ion current $I_{i_{meas}}$.

V. I-V CURVES

Current-voltage (I-V) characteristics give access to plasma parameters such as electron and ion temperature and densities[13,14,71]. In the case of a Faraday cup, ion current saturation ($I_{i_{sat}}$) can be accurately determined for a given position, see figure 9.

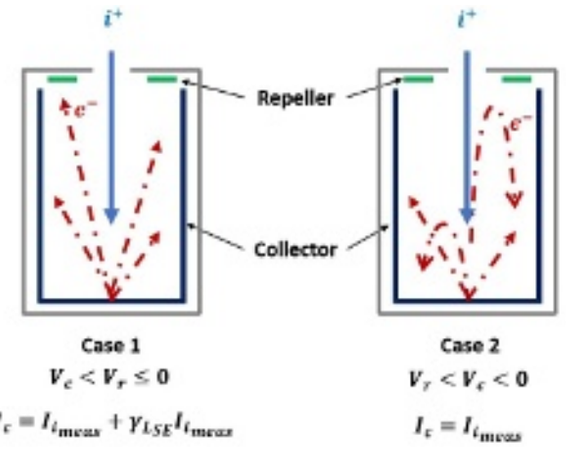

FIG. 8. Ion induced electron (SE) emission from Indium projectile escape (left) and recollection (right).

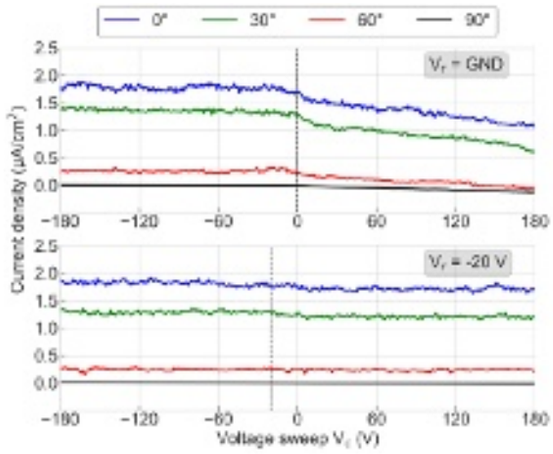

FIG. 9. Examples of I-V curves measured at 0, 30, 60 and 90. The repeller is either grounded (top) or biased to -20 V (bottom). The thruster fires at 2 mA, 7 kV and -7.4 kV.

First, the ion current density drops as the probe moves away from the thruster centreline. From 0 to 30 the ion saturation current density drops by ∼35%, as can be seen in figure 6. $I_{i_{sat}}$ is 100 times smaller at the edge of the thruster plume (90) than on axis (0). As expected j_i is larger at small angles in the vicinity of the thruster axis. Second, the measured current varies only on the positive branch of the I-V curve whatever the repeller potentials. But the change is weak when the collector is negatively biased. Third, there is no positive current measured for applied voltage larger than 0 V. The absence of primary electron is a characteristic of FEEP thruster plumes when no neutraliser is used, therefore, the electron current contribution only originates from thermal electrons which is very small compared to the ion current.

Figure 10 is an enlargement of an I-V curve acquired on the thruster axis (0) with the FC configuration 50.Al.05.P. The collector ($V_{collector}$ or V_c) potential is swept while the repeller ($V_{repeller}$ or V_r) is biased to -100 V. The top plot represents the collector current while the bottom one shows the current

measured on the repeller. Both current acquisitions are done simultaneously. The dashed lines delimit three distinct zones:

1. In the case of $V_c < V_r < 0$, both electrodes measure an ion current. However, the current measured by the repeller is more than 10 times lower than the collector one.

2. At $V_r < V_c < 0$, a current drop occurs on the collector while the current measured by the repeller increases. It corresponds to a change of direction of SE produced by the collector. For $V_c < V_r < 0$, these electrons were collected by the repeller, but are now ($V_r < V_c < 0$) directed back to the collector.

3. When $V_r < 0 < V_c$ the collector current drops once more while the repeller current rises to reach magnitudes three times higher than in zone 2, but still remains 20 times smaller than what is measured on the collector. This new current variation is caused by thermal electrons in the vicinity of the probe aperture. Once the collector potential is above 0 (ground) it starts to collect any electrons that were shielded by the repeller in zone 1 and 2. The ion current measured on the repeller refers principally to thermal ions. A small fraction of this current is also due to reflected ions with low energies pushed back by the positive collector potential and therefore collected by the negative repeller[72].

According to figure 10, the closest current to the true ion current corresponds to the current measured by the collector in zone 2. Indeed, in zone 2 the current acquired by the collector (blue, top) accounts for the secondary electrons recollection (see section IV). Moreover, simultaneously the current measured by the repeller (red, bottom) only accounts for 2% of the total current entering the cup (blue and red curve) therefore, zone 2 can be considered to give the closest value to the real ion current. Note that the slope measured in zone 2 between -100 V and 0 is small enough (≈ -42 pA / V) to consider any voltage point to provide the correct ion current. Therefore, current density angular distribution measurement of an EP device shall be carried out with the FC following the condition : $V_r < V_c < 0$.

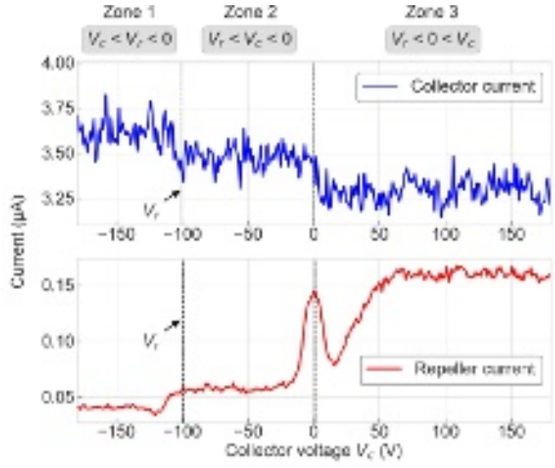

FIG. 10. Three current collection zones on thruster axis. V_r is fixed at -100 V. Current measured on the collector (top) and repeller electrode (bottom). The thruster fires at 2 mA, 7 kV and -7.4 kV

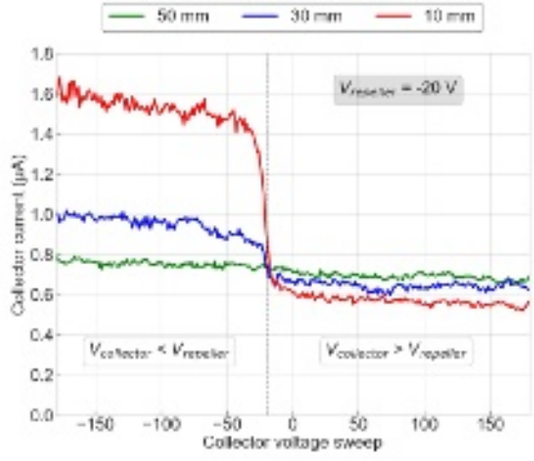

FIG. 11. IV curves corresponding to experiment described in Figure 8. A voltage sweep is applied to the collector while the repeller is biased to -20 V. The thruster fires at 2 mA and 7 kV. Designs 50.G.07.E (circle), 30.G.07.E (square) and 10.G.07.E (triangle) are studied.

VI. FARADAY CUP SE TRAPPING EFFICIENCY UNDER INDIUM ION IMPACTS

FC designs 50.G.07.E, 30.G.07.E and 10.G.07.E are studied in this section. I-V curves acquired on the thruster axis are used to get the ion current saturation (I_{isat}) as plotted in Figure 11. The repeller is biased to -20 V as represented by the dashed lines. When $V_c < V_r$, the shorter the cup the higher the ion current. In contrast, when V_c overtakes V_r the ion current is lower with a shorter cup. This behaviour is characteristic to SE recollection by the collector as explained in section IV and V. The slight difference in current when $V_c > V_r$ between the three probe designs can be due to changes in the thruster extractor voltage. Due to small impedance variations the total discharge voltage had to be adapted to reach similar current and voltage emission conditions. In this case the extractor was at -6.8 kV, -7.1 kV and -7.4 kV for 50 mm, 30 mm and 10 mm respectively. When the extractor voltage increases, the thruster ion current angular distribution gets wider which decreases the ion current on the thruster axis (VII B). However, the gap between 10 mm FC and the two other cups is too large to be only caused by extractor potential variations. The 10 mm long FC might be too short to recollect all reflected primary ions.

Figure 12 shows three plots. The first two represent angular current density distributions with (middle) and without (top) SE recollection. When SE are recollected, it means the current is acquired in zone 2 introduced by figure 10 in section V. On the opposite, when SE are not recollected, the current is acquired in zone 1. The third plot displays the angular de-

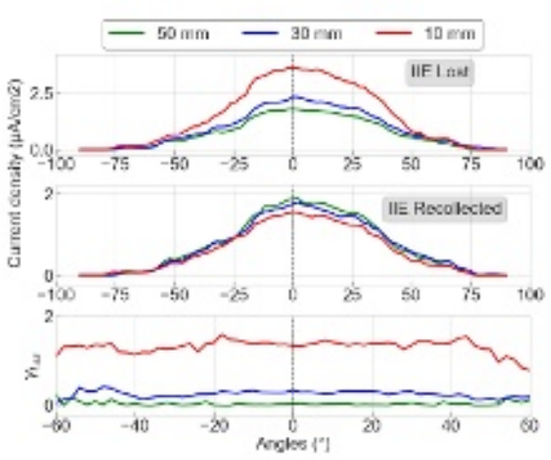

FIG. 12. Ion current densities profile of the laboratory thruster measured with cup of 10 mm, 30 mm and 50 mm long. Case of loss (top) and recollection (middle) of SE. The angular distribution of their respective γ_{SE} is plotted at the bottom. The thruster fires at 2 mA and 7 kV.

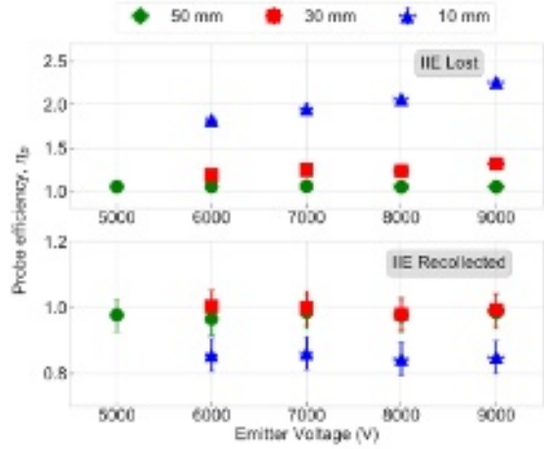

FIG. 13. Probe efficiency measured with different FC lengths. The thruster fires at 2 mA with 6 kV, 7 kV, 8 kV and 9 kV. $I_{i_{int}}$ is computed when all SE are escaping the cup (top) and when they are fully recollected (bottom)

pendency of $\gamma_{L_{SE}}$ for a given cup length. Here, the yield is computed using equation 10. Current acquired in zone 1 corresponds to $I_{i_{SE}}$ and the one measured in zone 2 is $I_{i_{meas}}$. We observe that the smaller the cup length the larger the yield. Moreover, $\gamma_{L_{SE}}$ does not seem to be dependent on the angular position of the Faraday cup. At large angles (>80) facilities effect are predominant, therefore the yield cannot be computed accurately. From the current density profiles the experimental ion current (I_{int}) is computed using equation 2. The probe efficiency η_p, equation 6 is determined and plotted in figure 13. Plots confirm that SE contribute to the experimental ion current if poorly recollected. The ion collection efficiency with a 50 mm Faraday cup shows no or limited dependency to indium ion energies. Note that almost all the ion current is collected whatever the configuration. With a 30 mm cup the experimental ion current is about 20% - 30% above the real current when SEs escape the cup. This configuration starts to be sensitive to high ion energies as well. With a 10 mm cup the I_{int} is up to 120% above the real current with no SE recollection.When SE are properly captured the FC with 50 mm and 30 mm show similar collection efficiency. Furthermore, with the right electrode potentials the three FC efficiency become insensitive to incoming ion energy. Table IV gathers all $\gamma_{L_{SE}}$ measured with three different cup lengths and for different ion energies. The yield is given for a collector in aluminum foam.

From our results it is clear that the cup length of a FC is a critical parameter to reduce the effect of SE upon the measured ion current. We have nevertheless shown that with the right potential distribution the capture of SE is possible which makes smaller cup length ($\leq$30 mm) usable and reliable. For results shown in the next section the cup length is fixed to 50 mm.

VII. FARADAY CUP DESIGN OPTIMIZATION

TABLE IV. FC SE yield trapping for different cup lengths and ion energies. The collector is an aluminium foam.

Ion energy	$\gamma_{L_{SE}}$ **10 mm**	$\gamma_{L_{SE}}$ **30 mm**	$\gamma_{L_{SE}}$ **50 mm**
keV	#	#	#
6±0.06	1.16±0.058	0.21±0.01	0.03±0.002
7±0.07	1.37±0.068	0.27±0.013	0.03±0.002
8±0.08	1.49±0.074	0.28±0.014	0.03±0.002
9±0.09	1.72±0.086	0.37±0.018	0.03±0.002

A. Sputtering and propellant deposition

In the case of Faraday cups a large fraction of the flux is concentrated on the front and on the ion collector. With standard designs the front of a FC is the repeller (also called collimator in the literature). Figure 14 shows the ion collection efficiency (η_p) of Faraday cups with different repeller materials exposed to the ion beam (top). Graphite (50.G.05.E), molybdenum (50.Mo.05.E) and aluminium (50.Al.05.E) were chosen for the front of the probe. Graphite is known for its low sputtering yield, molybdenum is often used in plasma diagnostics designs and aluminum is cheap and easy to obtain while still being suitable for low-power EP plume study. The bottom plot in figure 14, shows the ion collection efficiency with aluminum used for the front with configuration 50.Al.05.E and 50.Al.05.P as introduced in figure 5. For both studies the thruster fires at 2 mA and 7 kV. Data acquisition is done with the Faraday cup measuring in zone 1.
First, in the case where the repeller is exposed to the ion beam, we observe a decrease of collection efficiency between graphite, molybdenum and aluminium. The same behaviour was noted in a publication related to FC optimization for Hall Thruster[72]. The efficiency drop between FC 50.G.05.E and 50.Al.05.P is only about 5%. As the uncertainty in our computation is in the order of 3% this difference can be con-

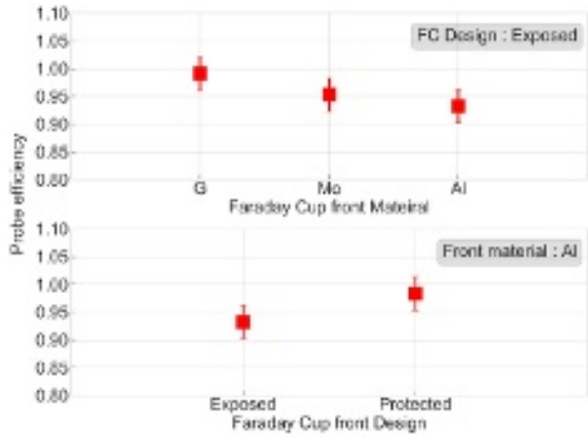

FIG. 14. FC ion collection efficiency for different probe front properties (top) and designs (bottom), as introduced in section II C, under indium ion bombardment. The Thruster fires at 2 mA and 7 kV.

sidered very small. Furthermore, we note that configuration 50.G.05.E measures 99±3% of the ion current. In the worst case, ie 50.Al.05.E, the probe still collects 94±3% of the emission current.

Second, on the bottom plot we observe a higher collection efficiency for FC configuration 50.Al.05.P when compared to FC 50.Al.05.E. When the repeller is protected from direct beam exposure the collection efficiency increases and 98±3% of the beam ion current is captured, a value close to the efficiency obtained with the configuration 50.G.05.E.

Using the housing front as collimator provides extra shielding for the collector. Moreover, with this configuration the cup top is positioned further away from the probe entrance which reduces the probability to collect electrons and SE produced close to the electrode by the probe front. Finally, indium is a liquid metal which tends to depose easily on material surfaces. Figure 15 shows different part of a Faraday cup after being exposed for a long time to the *ENPULSION NANO* beam. Parts which are constantly exposed to the thruster plume, i.e. repeller and housing front, show no trace of propellant deposition. Coating on these surfaces are directly removed by high energy ions. However, the side part of the FC and the insulator located between the repeller and housing front present a thin layer of deposition. Accumulation of propellant deposition on the insulator leads to FC failure either due to current leak or caused by short circuit between the repeller and the grounded housing. With configuration X.X.X.P only the housing front will be exposed. There, ions will either be directly collected by the collector or be removed by other ions if a thin layer accumulates on the housing front.

From this study, we consider a FC in configuration X.X.X.P is the most reliable design. With this configuration a FC is less impacted by the front material. In addition, it strongly reduces deposition on the probe parts.

B. Collection area definition

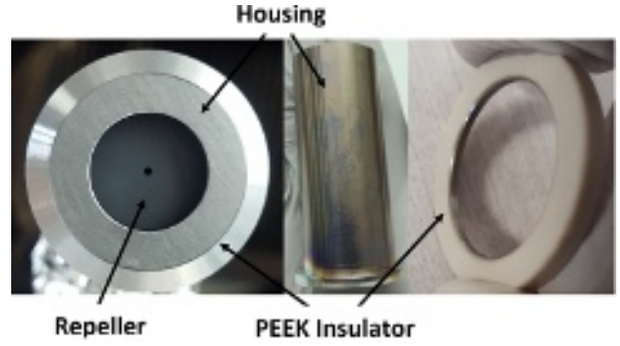

FIG. 15. Indium propellant deposition on insulator.

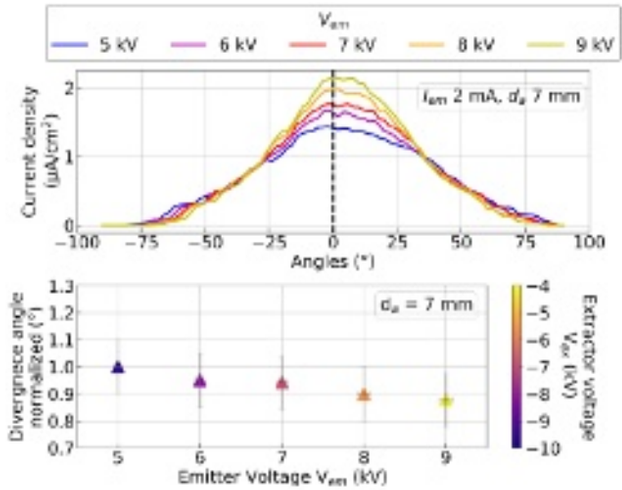

FIG. 16. Current densities angular distribution (J_i) with fixed Faraday cup geometry (d_a = 7 mm) and ion emission (I_{em}) for different acceleration potential (top). The corresponding divergence angle (θ_{div}) is plotted at the bottom.

The collection area used to integrate the current density in equation 1 is given by the smallest diameter of the probe assembly. The need to carefully design the probe front in terms of materials properties and beam exposure was previously explained. The front aperture diameter d_a of a FC is of great importance since it collimates the ion flux flowing through the collector. To define the optimized aperture dimension when studying the plume of a low power FEEP thruster, configuration 50.G.10.E, 50.G.07.E, 50.G.05.E, 50.G.03.E and 50.G.01.E have been tested.

First, the impact of thruster firing parameters such as acceleration potential and total discharge voltage for a fixed emission current was examined (Mode 1). The first plot in figure 16 shows the *ENPULSION NANO* plume profile measured for emitter voltage from 5 kV to 9 kV with configuration 50.G.07.E. To keep the emission current constant the total discharge voltage must be adjusted via the extractor potential. When V_{em} increases V_{ex} decreases which focus the beam and step the ion density up on the thruster axis. The opposite behaviour happens when V_{em} decreases.

The evolution of corresponding θ_{div} is displayed on the sec-

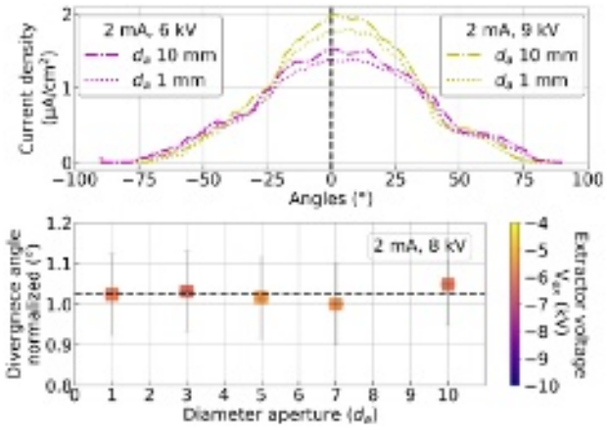

FIG. 17. Top: current density angular distribution (J_i) with $d_a = 10$ and 1 mm with thruster operated at 2 mA, 6 kV (purple) and 9 kV (yellow). Bottom: evolution of θ_{div} computed with different FC diameter with the thruster firing at 2 mA and 8 kV.

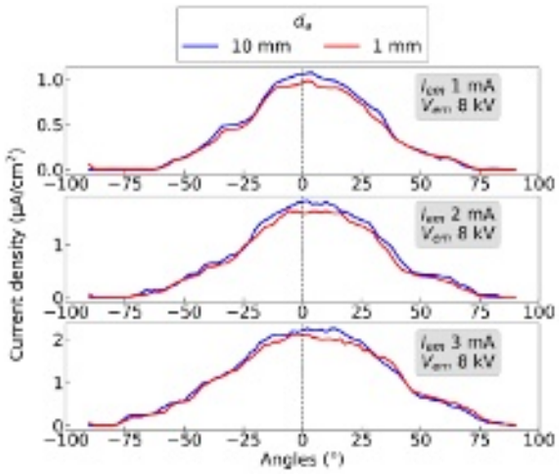

FIG. 18. Current density angular distribution (J_i) with fixed acceleration potential (8 kV) for different ion emission current 1 mA (top), 2 mA (middle), 3 mA (bottom). Profiles are measured with configuration 50.G.10.E (blue) and 50.G.01.E (red).

ond graphic. On the y-axis, 1 corresponds to θ_{div} obtained when the thruster fires at 2 mA and 5 kV. All values are normalized to better show the overall evolution of the beam divergence when the emitter and extractor voltages increases and decreases, respectively. We observe a relatively small decrease between the largest and smallest extractor voltage.

Figure 17 displays the ion current density angular distribution measured with configuration 50.G.10.E and 50.G.01.E. Here, the thruster fires at 2 mA, 6 kV (purple) and 9 kV (yellow). The Faraday cup with an aperture diameter of 1 mm gives less current density compared to the 10 mm one. The difference slightly increases when the emitter voltage raises. The variation between the two configurations is 10±0.7% and 12±1.4% with standard deviation around 5% for low and high emitter voltage, respectively. The bottom plot gives the evolution of θ_{div} computed with different FC aperture diameter. The thruster fires at 2 mA and 8 kV. Despite the ion signal difference observed between the largest and the smallest d_a the corresponding θ_{div} remains constant. There is no relation between the divergence angle and the aperture diameter of the FC.

Similarly, the current density angular distributions when the thruster fires in mode 2 (see table I) are plotted in figure 18. Configuration 50.G.10.E and 50.G.01.E are used once more. Similar observations show that a FC configuration with aperture diameter of 1 mm collects less ion current density. The variation is again near 10% for each thruster operation point. Therefore, we understand that the ion current density variation when d_a varies depends on the potential applied to the extractor (V_{ex}) rather than on the emission current and voltage.

This statement is strengthened by results displayed in figure 19. η_p is computed from ion current density measured with FC 50.G.05.E (VII A). In section VI, proofs were given that η_p is barely impacted by changes of ion energies when the cup is 50 mm long. In figure 19 the ion current is acquired in zone 1 (see section V). Therefore, efficiencies are not corrected with the coefficient experimentally found in table IV. Values

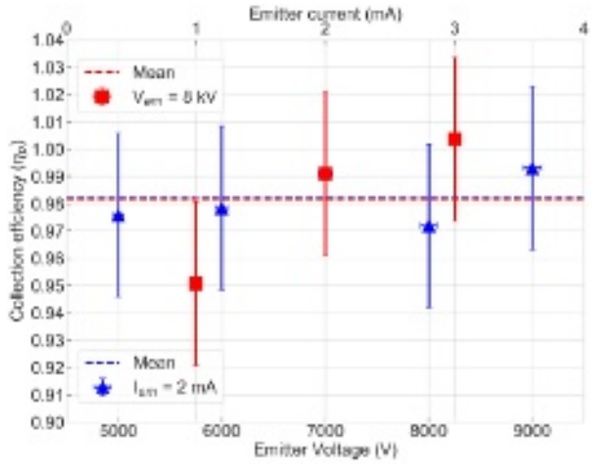

FIG. 19. Probe collection efficiency of a Faraday cup in configuration 50.AL.05.P. The thruster is firing at 2 mA with different emitter voltage (blue) and at 8 kV with different emitter current (red)

are displayed when the thruster fires in mode 1 (blue) and 2 (red). We note that as expected the current intensity does not affect the collection efficiency. Indeed, efficiency variations are included in the uncertainties. Dashed lines represent the average of all value for mode 1 and 2. Mean probe efficiencies are similar with standard deviation below 2%.

To assess the impact of the ion signal losses observed when d_a is reduced η_p is plotted in figure 20. There, FC configurations with aperture diameter from 1 mm to 10 mm and a cup length of 50 mm are used. The thruster fires in mode 1. η_p decreases with the probe front diameter. Nevertheless, overall the probe efficiency drop is relatively small. In the worst case the efficiency drops by 10% when the aperture diameter is divided by 10. Such a behaviour was also observed in the plume of Hall thrusters[72]. Efficiency losses were more

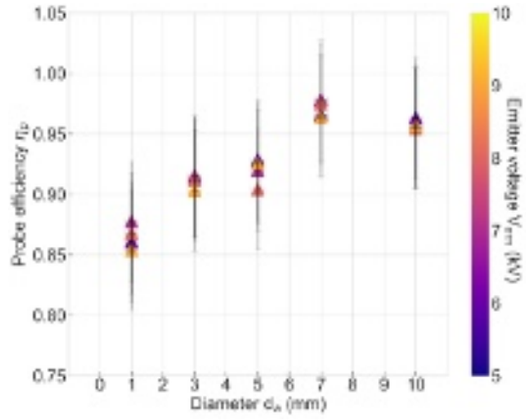

FIG. 20. Probe collection efficiency for different inlet aperture diameters. The thruster fires at 2 mA.

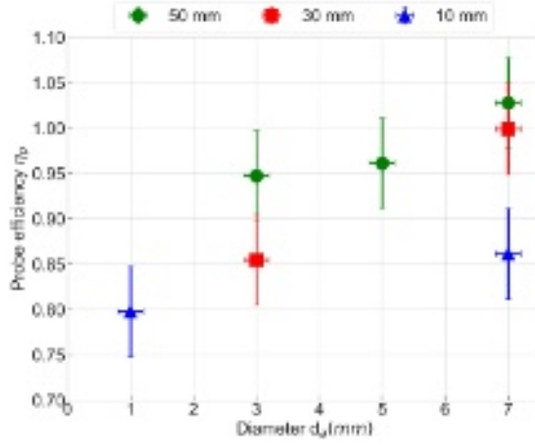

FIG. 21. Probe collection efficiency for different aperture diameters and cup lengths. The thruster fires at 2 mA and 7 kV.

important with the Hall thruster technology due to a complex plume structure. Identical experiments have been conducted with different cup lengths. Results are shown in figure 21. This time, the SE current contribution is suppressed. The ion collection efficiency η_p is given for FC configurations 50.G.X.E (green), 30.G.X.E (red) and 10.G.X.E (blue). Designs 50.Al.05.P, 30.G.03.E and 10.G.01.E share similar collection solid angle. For a given solid angle, η_p still decreases when the aperture diameter decreases. At d_a = 7 mm, η_p is close to 1 for both 50 mm and 30 mm cup length. However, once d_a is reduced to 3 mm , configuration with l_{cup} = 30 mm gives an ion collection efficiency around 8% lower than the FC with l_{cup} = 50 mm.

All experiments bring out the main factor for ion collection losses is the aperture diameter d_a. In the case of low power FEEP thrusters we recommend that d_a to be at least larger than 7 mm when the cup length is $\geq$30 mm.

VIII. CONCLUSION

This work aims to provide information about FC design to study the plume of a low power FEEP thruster. To obtain accurate measurement of ion currents one must follow several recommendations. First, we have demonstrated that the length of a FC cup is the main factor for SE recollection. The amount of SE not being captured by the cup is directly related to the cup length when no specific potential to the repeller and collector is applied (section VI). In the case of a low power FEEP thruster the ideal would be a cup length $\geq$50 mm. This parameter is of great importance for studying other EP technology plasma with ion energy in the order of few several volts. This way SEs could be properly recollected without modifying the probe field lines which could interact with ions flying through the cup. Second, the collection area definition influences the ion current density measured. At constant distance from the thruster we observed a decrease of the ion current density when d_a decreases (section VII B). In our case study an inlet aperture diameter of 7 mm is sufficient to properly measure the ion current. Third, a FC shall sustain long duration operation. Therefore, coating formation and material sputtering shall be minimized. Moreover, the collector shall be properly shielded against non desired particles originating from plasma-probe interactions. We proposed a configuration (section VII A) where the front of the probe is used to collimate the ion flux, preventing any deposition on critical insulation part of the probe. Moreover, this leaves room to use the repeller, placed behind, to prevent SEs emitted by the probe front to be captured by the collector. The last step is to find the right operation settings for the probe. This can be achieved with IV characterizations that allow to determine the collector bias (V_c) and the repeller potential (V_r). V_c is set to only collect ions and prevent to capture plasma or thermal electrons and V_r must fulfil the condition $V_r \leq V_c$. This way SE from the collector can be recollected and $I_c = I_i$ (section V). Study presented in appendix shows that with an optimized design a FC can be a powerful tool to determine thruster performance parameters such as beam divergence, efficiency, beam deviation and thrust. Nevertheless, FC design and recommendation remain to be verify with other EP technologies with e.g. higher ion current densities, lower ion energies and more complex plumes.

ACKNOWLEDGMENTS

Part of this research is financially supported by the ESA, ESTEC under grant PO-5401003120, and by the ENPULSION company. Authors would like to thank Dr. Pr. Aumayr for his support on theoretical subject regarding plasma diagnostics design and behaviour. Additionally, we would like to thank Dr. Scharlemann head of the FH Wiener Neustadt Aerospace department for putting their facilities to our disposition to conduct our experiments as well as FOTEC Forschungs-und Technologietransfer GmbH for their technical support.

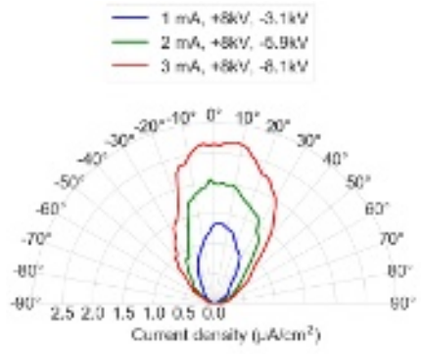

FIG. 22. Beam profiles in polar coordinate of the laboratory unit ENPULSION NANO firing at 1 mA, 2 mA and 3 mA with an emitter voltage fixed at 8 kV. The Faraday cup configuration is 50.Al.07.P with a foam #4 collector.

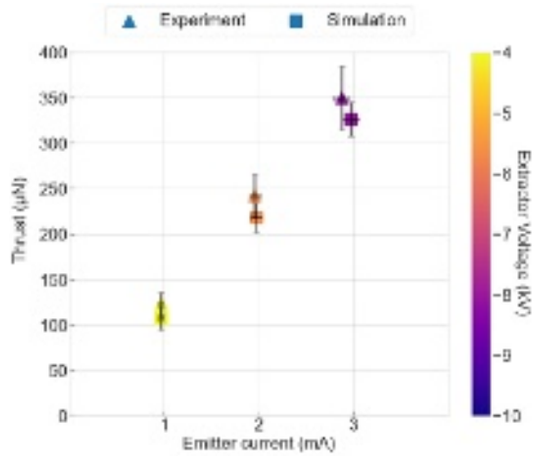

FIG. 23. Experimental (FC measurements) versus numerical thrust for the laboratory unit ENPULSION NANO. The thruster is firing at 1 mA, 2 mA and 3 mA with an emitter voltage fixed at 8 kV. The FC is in configuration 50.Al.07.P with a foam #4 collector.

Appendix: Experimental vs numerical thrust.

The accuracy, reliability and robustness of our FC design were demonstrated in previous sections. Based on preliminary work it is possible to select the best FC configuration to compute the thrust. Data sample are measured with FC configuration 50.Al.07.P. The thruster fires in mode 2. Beam profiles acquired with the FC are displayed in figure 22. A polar scale is used to ease profile visualization. We observe a slight tilt of the beam mainly caused by the distribution of emitter crown injectors. The planar deviation ζ can be calculated as described in section III A. It goes from $\sim$2 to 3 between 1 mA and 3 mA. The thrust is computed as a scalar. The effective divergence angle λ, which accounts for momentum losses, is used to find the thrust loss factor F. Then, T is computed using equation 5. Figure 23 shows thrust values found experimentally (triangle) and numerically[45] (square) as explained in section III B. Experimental data uses $I_{i_{int}}$ while the simulation rely on recorded emission current I_{em}. On the right side, the extractor voltage is given for each firing steps. There is a relatively good agreement between experimental data and outcomes of the mathematical model. Nevertheless, the experimental thrust is always higher. The deviation reaches $\sim$15% at low emission current and goes down to $\sim$7.5% for high current operation. Considering the uncertainties and knowing that both experimental and model methods are indirect thrust measurements one cannot be sure which method is the most accurate.

DATA AVAILABILITY

Plume data obtained in the frame of this study are available upon request. Contact the corresponding author. Data about the *ENPULSION NANO* thruster design are confidential.

[1]D.Selva and D.Krejci, "A survey and assessment of the capabilities of Cubesats for Earth observation," Acta Astronautica **74** (2012).
[2]J.N.Pelton, S.Madry, and S.Camacho-Lara, *Handbook of Satellite Applications*, springer ed., edited by M. S. C.-L. S. Pelton, Joseph N. (2017).
[3]P.Lascombes and H.David, "Electric Propulsion for Small Satellites Orbit Control and Deorbiting: The Example of a Hall Effect Thruster," in *SpaceOps Conferences* (2018).
[4]Levchenko, Keidar, Cantrell, Wu, Kuninaka, Bazaka, and Xu, "Explore space using swarms of tiny satellites," Nature **562** (2018), 10.1038/d41586-018-06957-2.
[5]D.Lev, R.M.Myers, K.M.Lemmer, J.Kolbeck, H.Koizumi, and K.Polzin, "The technological and commercial expansion of electric propulsion," **159** (2019), 10.1016/j.actaastro.2019.03.058.
[6]A.W.Hanson, "Satellite Internet in the Mobile Age," New Space **4** (2016), 10.1089/space.2016.0019.
[7]D.M.Goebel and I.Katz, *Fundamentals of Electric Propulsion: Ion and Hall Thrusters*, jet propulsion laboratory, california institute of technology ed. (2008) p. 493.
[8]S.Mazouffre, "Electric propulsion for satellites and spacecraft: established technologies and novel approaches," Plasma Sources Science and Technology **25**, 27 (2016).
[9]K.Lemmer, "Propulsion for CubeSats," Acta Astronautica **134** (2017).
[10]D.Krejci and P.Lozano, "Space Propulsion Technology for Small Spacecraft," in *Proceedings of the IEEE* (IEEE, 2018).
[11]I.Levchenko, S.Xu, S.Mazouffre, D.Lev, D.Pedrini, D.Goebel, L.Garrigues, F.Taccogna, and K.Bazaka, "Perspectives, frontiers, and new horizons for plasma-based space electric propulsion," Physics of Plasmas **27** (2020).
[12]C.M.Marerese, N.Majumdar, J.M.haas, G.Williams, L.B.King, and A.D.Gallimore, "Development of a single-orifice Retarding Potential Analyser for Hall Thruster Plume Characterization," in *25th International Electric Propulsion Conference* (1997).
[13]Sheridan, "How big is a small Langmuir probe," Physics of Plasmas (2000).
[14]V.I.Demidov, S.V.Ratynskaia, and K.Rypdal, "Electric probes for plasmas, the link between theory and instrument," Review of scientific instruments **73** (2002).
[15]F.F.Chen, *Mini course on Plasma Diagnostics (Langmuir probes)*, Electrical Engineering Department University of California, Los Angeles (2003).
[16]R.L.Merlino, "Understanding Langmuir probe current-voltage characteristics," J.Phys (2007).
[17]I.Korolov, *Theory and application of Langmuir probes*, Greifswald (2010).
[18]K.J.Terhune and L. King, "Ion and Mass Measurement of an ELectrospray Emitter using ExB filter," in *32nd International Electric Propulsion Conference* (2011).
[19]J.P.Sheehan and N.Hershkovitz, "Emissive probes," Plasma Sources Science and Technology (2011).

[20]N.Teshigahara, S.Shinohara, Y. Yamagata, D. Kuwahara, and M. Watanabe, "Development of 2D Laser-Induced Fluorescence (LIF) System in High-Density Helicon Plasma," Plasma and Fusion Research **9** (2014).
[21]B.S.Rawat, S.Vala, M.Abhangi, R.Kumar, and S.Chauhan, "Design and simulation of 10kW Faraday cup for ion beam current," in *25th International Conference on Nuclear Engineering ICONE25* (2017).
[22]S.Mazouffre, G.Largeau, L.Garrigues, C.Boniface, and K.Dannenmayer, "Evaluation of various probe designs for measuring the ion current density in a Hall thruster plume," in *35th International Electric Propulsion Conference* (2017).
[23]D.L.Brown, M.L.R.Walker, J.Szabo, W.Huang, and J.E.Foster, "Recommended Practice for Use of Faraday Probes in Electric Propulsion Testing," Journal of Propulsion and Power **33** (2017).
[24]B.Vincent, "Incoherent Thomason scattering investigations in Hall thruster, planar magnetron and ECR ion source plasmas," (2019).
[25]J.Harasimowicz and C.P.Welsch, "Faraday cup for Low-Energy, Low-intensity Beam Measurements at the USR," in *Beam Instrumentation Workshop* (2010).
[26]J.Vaudolon, "Electric field determination and magnetic topology optimization in Hall thrusters," (2015).
[27]L.Grimaud, "Magnetic shielding topology applied to low power Hall Thrusters," (2018).
[28]T.Hallouin and S.Mazouffre, "Far-Field Plume Characterization of a 100-W Class Hall Thruster," Aerospace (2020).
[29]Z.Zhang, H.Tang, Z.Zhang, J.Wang, and S.Cao, "A retarding potential analyzer design for keV-level ion thruster beams," Review of Scientific Instruments (2016).
[30]N.Mühlich, S.Keerl, W.Engel, E.Ceribas, and R-J.Koopmans, "Retarding Potential Analyser Development for Low Density FEEP Thruster Beam Diagnostics," in *36th International Electric Propulsion Conference* (2019).
[31]J.L.Rovey, M.L.R.Walker, A.D.Gallimore, and P.Y.Peterson, "Magnetically Filtered Faraday Probe for Measuring the Ion Current Profile of a Hall Thruster," Reveiw of Scientific instruments **77** (2006).
[32]D. Renaud, D. Gerst, S. Mazouffre, and A. Aanesland, "EB probe measurements in molecular and electronegative plasmas," Research of Scientifique Instrument **86** (2015), 10.1063/1.4937604.
[33]R.L.Schuch and J.G.Kelly, "A Compact Faraday Cup Array for Measurement of Current Distribution from Pulsed Electron Beams," Review of Scientific Instruments **43** (1972), 10.1063/1.1685854.
[34]A.Bol, P.Leleux, P.Lipnik, P.Macq, and A.Ninane, "A novel design for a fast intense neutron beam," Nuclear Instruments and Methods in Physics Research **214** (1983), 10.1016/0167-5087(83)90582-3.
[35]R.R.Hofer, M.L.R.Walker, and A.D.Gallimore, "A Comparison of Nude and Collimated Faraday Probes for Use with Hall Thrusters," in *27th International Electric Propulsion Conference* (2001).
[36]L.Habl, D.Rafalskyi, and T.Lafleur, "Ion beam diagnostic for the assessment of miniaturized electric propulsion systems," Review of Scientific Instruments (2020), 10.1063/5.0010589.
[37]D.L.Brown and A.D.Gallimore, "Evaluation of ion collection area in Faraday probes," Rev. Sci. Instrum. **81**, 063504 (2010).
[38]D.L.Brown and A.D.Gallimore, "Evaluation of facility effects on ion migration in a Hall thruster plume," J. Propul. Power **27**, 573–585 (2011).
[39]I.Vasiljevich, M.Tajmar, W.Grienauer, F.Plesescu, N.Buldrini, J. D. Amo, B.Carnicero-Dominguez, and M.Betto, "Development of an Indium mN-FEEP Thruster," in *44th AIAA/ASME/SAE/ASEE Joint Propulsion Conference and Exhibit* (2008).
[40]R. R. N. A. D.Jelem, B.Seifert, "Performance mapping and qualification of the IFM Nano thruster EM for in orbit demonstration," in *53rd AIAA/SAE/ASEE Joint Propulsion Conference* (2017).
[41]D.Jelem, A.Reissner, B.Seifert, N.Buldrini, L.Wilding, and D.Krejci, "Direct thrust and plume divergence measurements of the IFM Nano Thruster," Advances in Space Research **62**, 3398–3404 (2018).
[42]S.Keerl, W.Engel, N.S.Mühlich, J.Fries, and B.Seifert, "Two-dimensional plasma plume density characterisation of the IFM Nano Thruster," in *36th International Electric Propulsion Conference* (2019).
[43]A.Reissner, N.Buldrini, B.Seifert, T.Hörbe, and F.Plesescu, "Testing and Modelling of the mN-FEEP Start-Up Performance," in *34th International Electric Propulsion Conference* (2015).
[44]D.Krejci and A.Reissner and T.Schoenherr and B.Seifert and Z.Saleem and R.Alejos, "Recent flight data from IFM Nano Thrusters in a low earth orbit," in *36th International Electric Propulsion Conference* (2019).
[45]D.Krejci, V.Hugonnaud, T.Schönherr, B.Little, A.Reissner, Q.Koch, E.Bosch Borràs, and J.González Del Amo, "Full Performance Mapping of the IFM Nano Thruster including Direct Thrust Measurements," Journal of Small Satellites **8**, 881–893 (2019).
[46]S.Marcuccio, A.Genovese, and M.Andrenucci, "Experimental Performance of Field Emission Microthrusters," Journal of Propulsion and Power **14** (1998).
[47]A. Genovese, W.Steiger, and M. Tajmar, "Indium FEEP microthruster: Experimental characterization in the 1-100μN range," in *37th AIAA/ASME/SAE/ASEE Joint Propulsion Conference and Exhibit* (2001).
[48]M.Tajmar, A.Genovese, and W.Steiger, "Experimental Performance of Field Emiision Microthrusters," Journal of Propulsion and Power **20** (2004).
[49]A.Genovese, N.Buldrini, M.Tajmar, E.Tamas, I.Vasiljevich, and K.Marhold, "Development of an Indium mN-FEEP Thruster," in *41st AIAA/ASME/SAE/ASEE Joint Propulsion Conference and Exhibit* (2005).
[50]I.Vasiljevich, N.Buldrini, F.Plesescu, M.Tajmar, M.Betto, and J. D. Amo, "Porous Tungsten Crown Multiemitter Testing Programmes Usin Three Different Grain SIzes and Sintering Procedures," in *The 32nd International Electric Propulsion Conference* (2011).
[51]G.I.Taylor, "Desintegration of water drops in an electric field," Royal Society **280** (1964).
[52]J. L. Mora and I. Loscertales, "The current emitted by highly conducting Taylor cones," Journal of Fluid Mechanics **260** (1994).
[53]M.Tajmar, C.Scharlemann, A.Genovese, N.Buldrini, W.Steiger, and I.Vasiljevich, "Liquid-metal-ion source development for space propulsion at ARC," Ultramicroscopy **109** (2009).
[54]T.Schoenherr and B.Little and D.Krejci and A.Reissner and B.Seifert, "Development, Production, and Testing of the IFM Nano FEEP Thruster," in *36th International Electric Propulsion Conference* (2019).
[55]A.Bulit, J. Luna, J. D. Ámo, B.Lotz, D. Feili, and H.Leiter, "Field-Emission-Electric-Propulsion (FEEP) plasma modeling: 3-D full particle simulations," in *35th AIAA/ASME/SAE/ASEE Joint Propulsion Conference and Exhibit* (1999).
[56]A.Passaro, A.Vicini, and L.Biagioni, "Plasma Thruster Plume Simulation: Effect of Vacuum Chamber Environment," in *35th AIAA Plasmadynamics and Lasers Conference* (2004).
[57]N.S.Mühlich, B.Seifert, and F.Aumayr, "Ifm nano thruster performance studied by experiments and numerical simulations," Journal of Physics D: Applied Physics (2020).
[58]M.S.Benilov, "The Child–Langmuir law and analytical theory of collisionless to collision-dominated sheath," Plasma Sources Sci. Technol. **18**, 14 (2008).
[59]M.Ye, Y.He, S.Hu, R.Wang, and T. et al., "Suppression of secondary electron yield by micro-porous array structure," Journal of Applied Physics **113** (2013).
[60]C.Swanson and I.Kaganovich, "Modeling of reduced secondary electron emission yield from a foam or fuzz surface," Journal of Applied Physics **123** (2018).
[61]C.Huerta, M.I.Patino, and R.E.Wirz, "Secondary electron emission from textured surfaces," Journal Physics D:Applied Physics **151** (2018).
[62]A.Ottaviano, S.Banerjee, and Y.Raitses, "A rapid technique for the determination of secondary electron emission yield from complex surfaces," Journal of Applied Physics **126** (2019).
[63]E.Huerta and E.Wirz, "Ion-induced electron emission reduction via complex surface trapping," AIP advances **9** (2019).
[64]Exxentis, "Exxentis Website Homepage,".
[65]V.Hugonnaud, S.Mazouffre, D.Krejci, B.Seifert, and C.Scharlemann, "Faraday cup design for low power electric thrusters," in *Space Propulsion 2020+1* (2021).
[66]D.L.Brown, A.W.Larson, and B.E.Beal, "Methodology and Historical Perspective of a Hall Thruster Efficiency Analysis," Journal of Propulsion and Power **25** (2009).
[67]M.Tajmar, W.Steiger, and A.Genovese, "Indium FEEP Thruster Beam Diagnostics, Analysis and Simulation," in *37th AIAA/ASME/SAE/ASEE Joint Propulsion Conference and Exhibit* (2001).
[68]D.Brown, "Investigation of low discharge voltage Hall Thruster characteristics and evaluation of loss mechanisms," (2009).
[69]F.G.Rüdenauer, H.M.Fehringer, A.Sieber, and W.Stieger, "Behaviour of Backsputterred Contaminations on Liquid Metal Indium Ion Emitters,".

[70]R.I.Hornsey, "The emission characteristics of an indium needle-type liquid metal ion source," Applied Physics A **49** (1989).
[71]J.D.Johnson and A.J.T.Holmes, "Edge effect correction of small planar Langmuir probes," AIP (1990).
[72]V.Hugonnaud and S.Mazouffre, "Optimization of a Faraday cup collimator for electric propulsion device beam study: Case of a Hall thruster," Applied Sciences (2021).

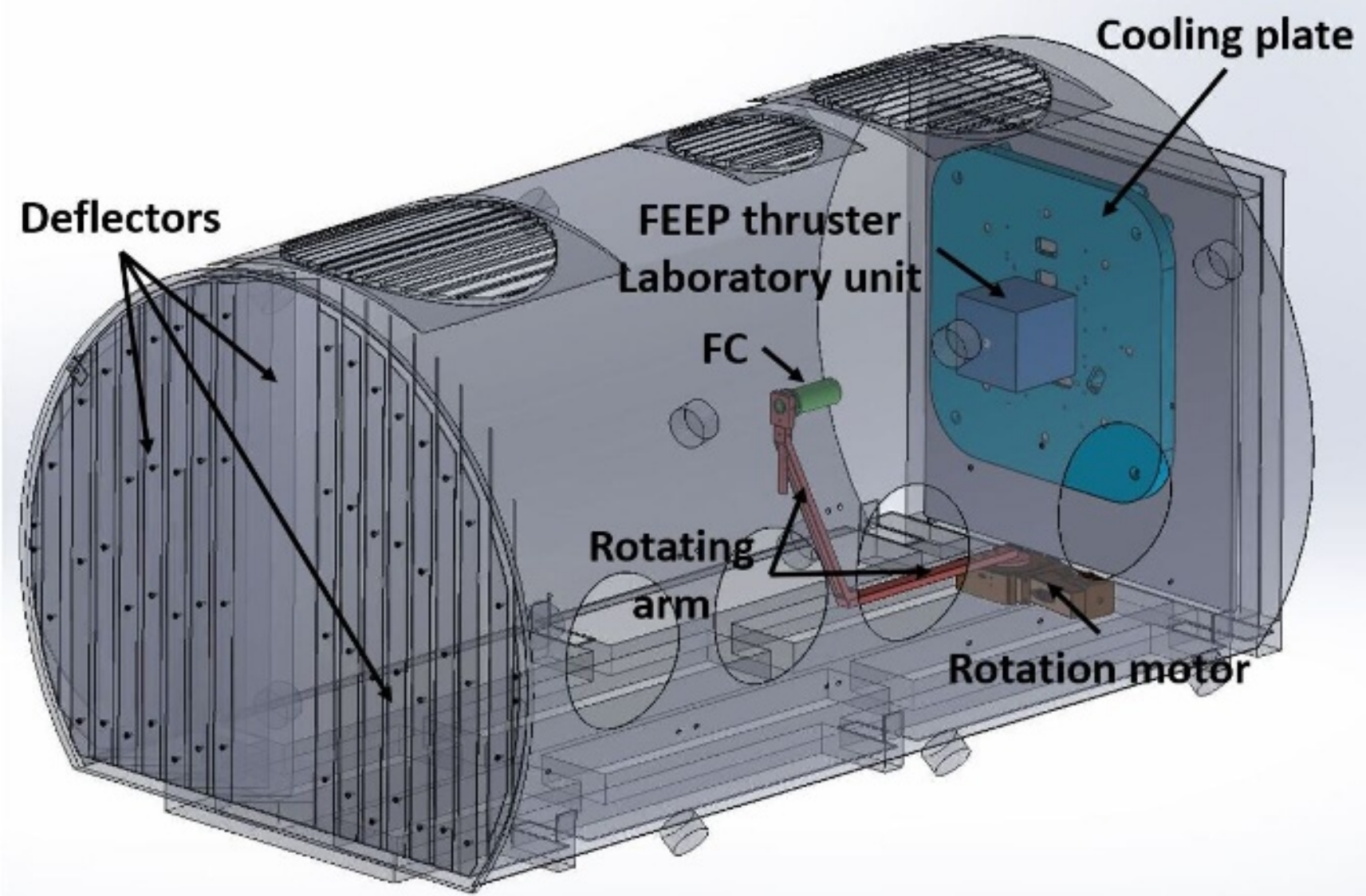
Cooling plate
Deflectors
FEEP thruster
Laboratory unit
FC
Rotating
arm
Rotation motor

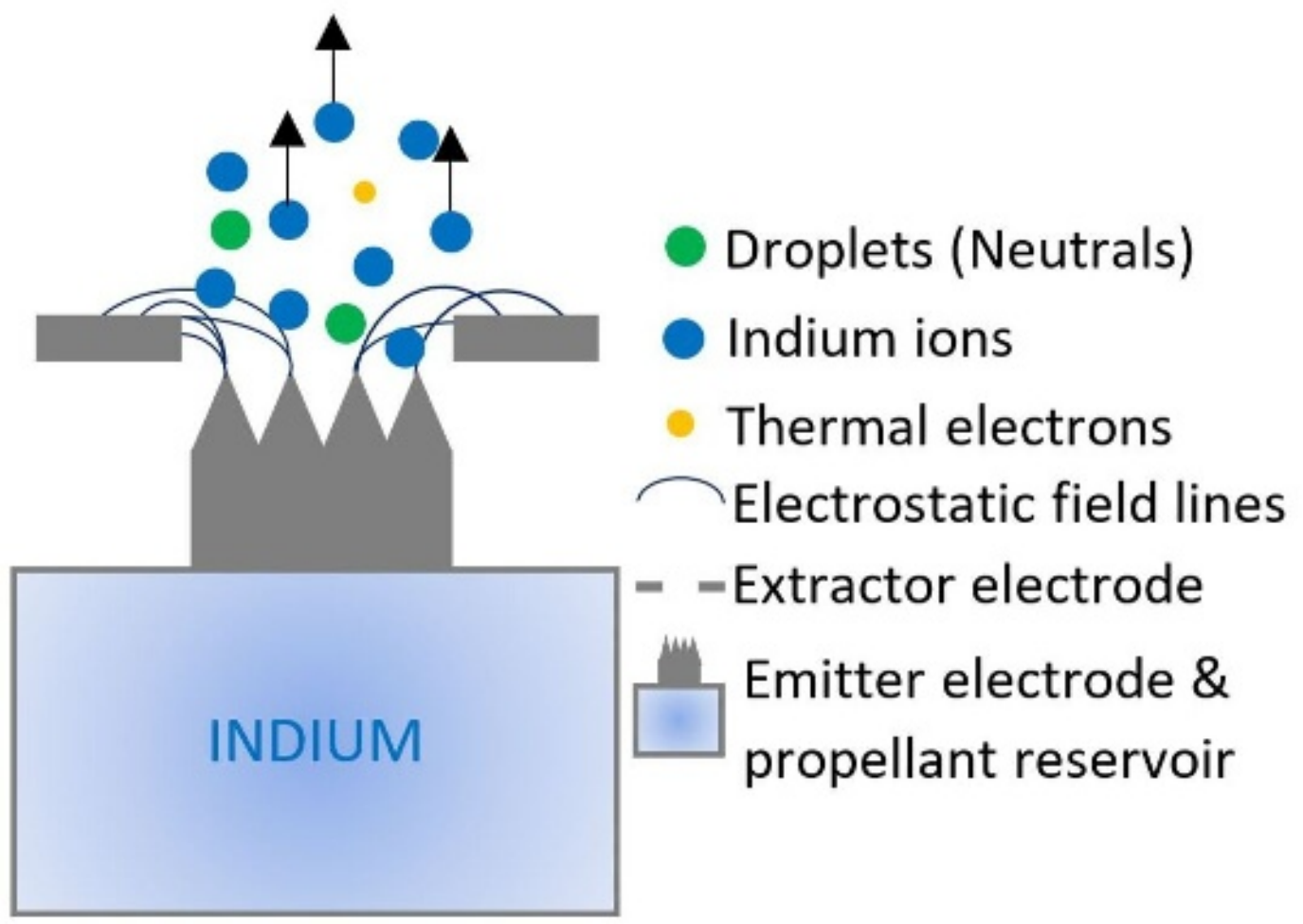
INDIUM
Droplets (Neutrals)
Indium ions
Thermal electrons
Electrostatic field lines
Extractor electrode
Emitter electrode &
propellant reservoir

FEEP
Laboratory Unit
Crown

A: Housing, B: Collimator or Repeller, C: Collector

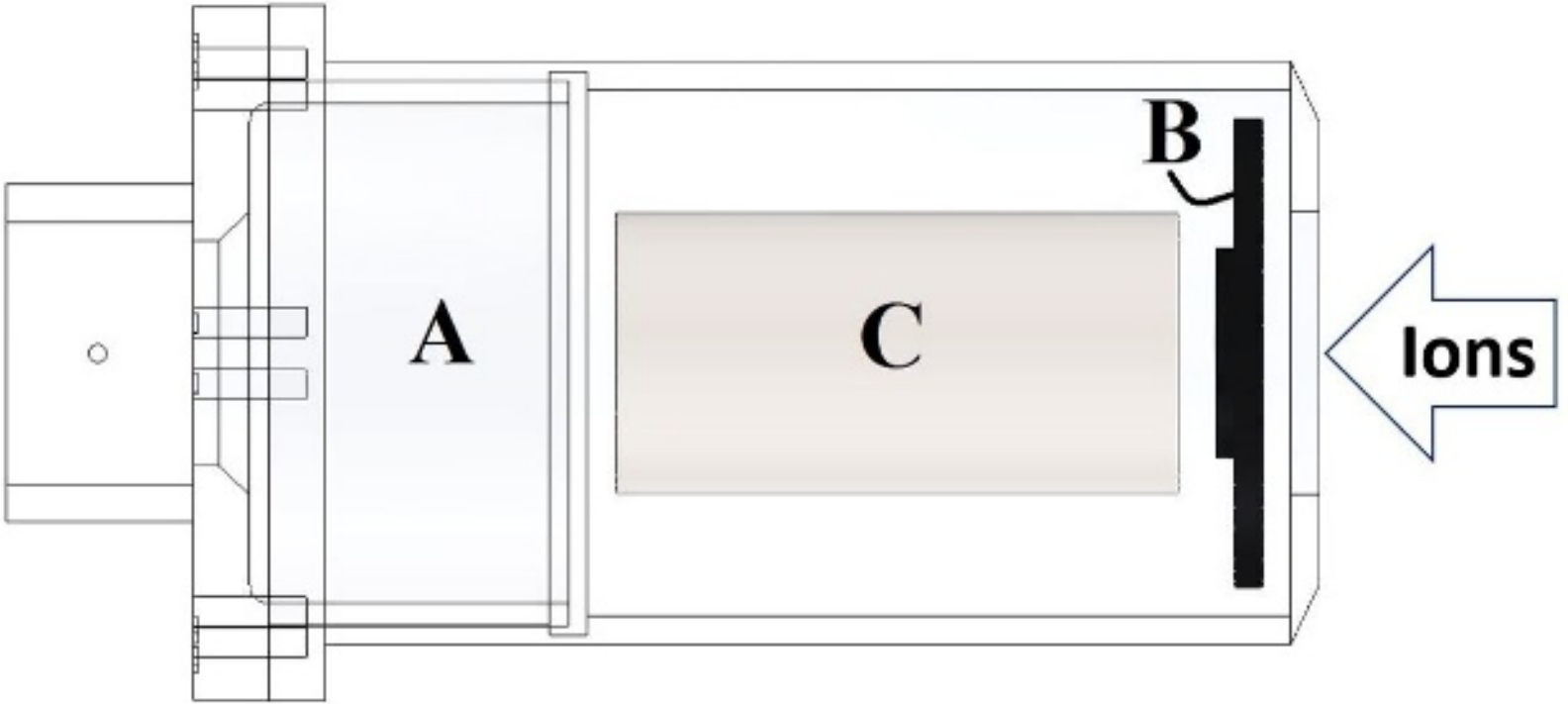

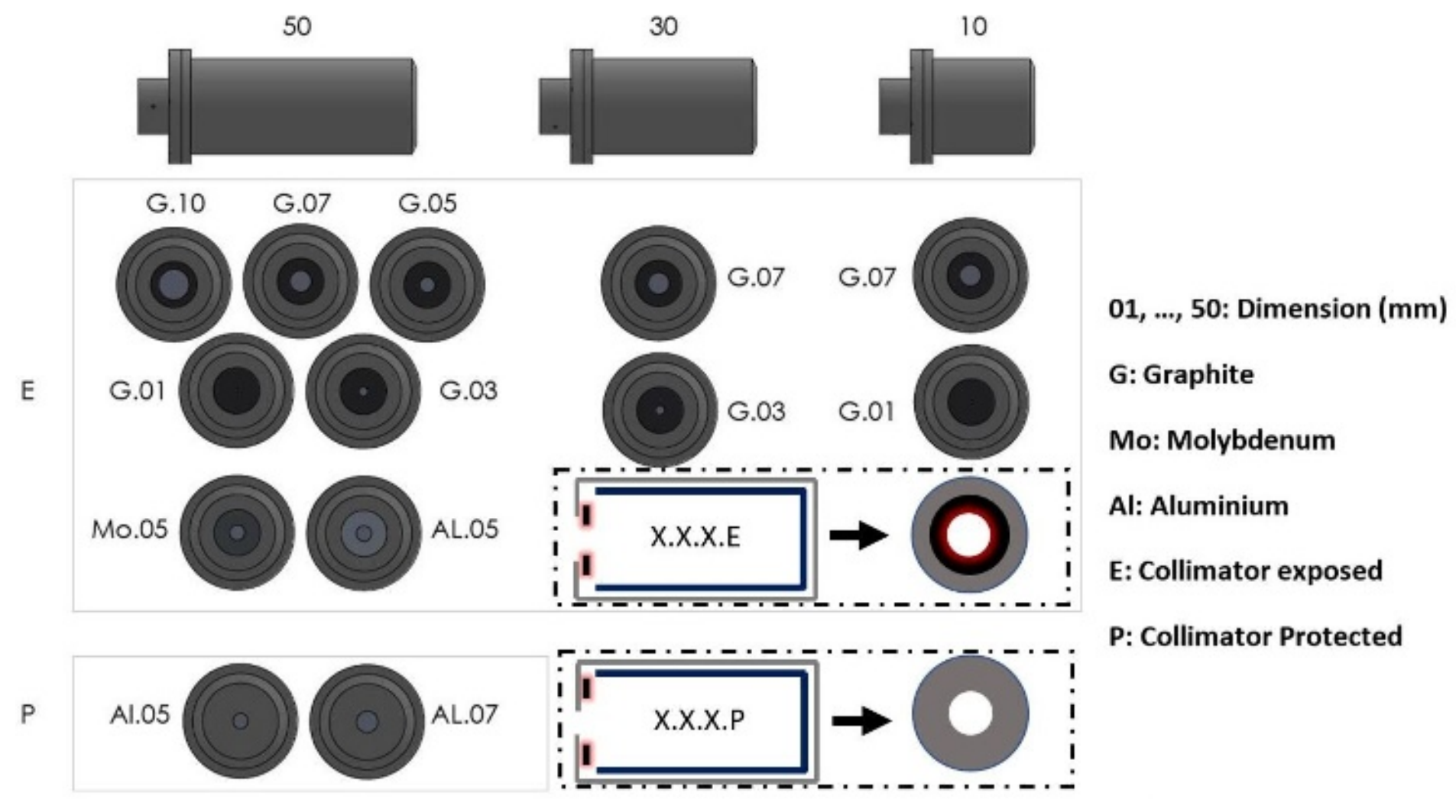
50
30
10
G.10
G.07
G.05
G.01
G.03
Mo.05
AL.05
G.07
G.07
G.03
G.01
X.X.X.E
E
Al.05
AL.07
X.X.X.P
P
01, ..., 50: Dimension (mm)
G: Graphite
Mo: Molybdenum
Al: Aluminium
E: Collimator exposed
P: Collimator Protected

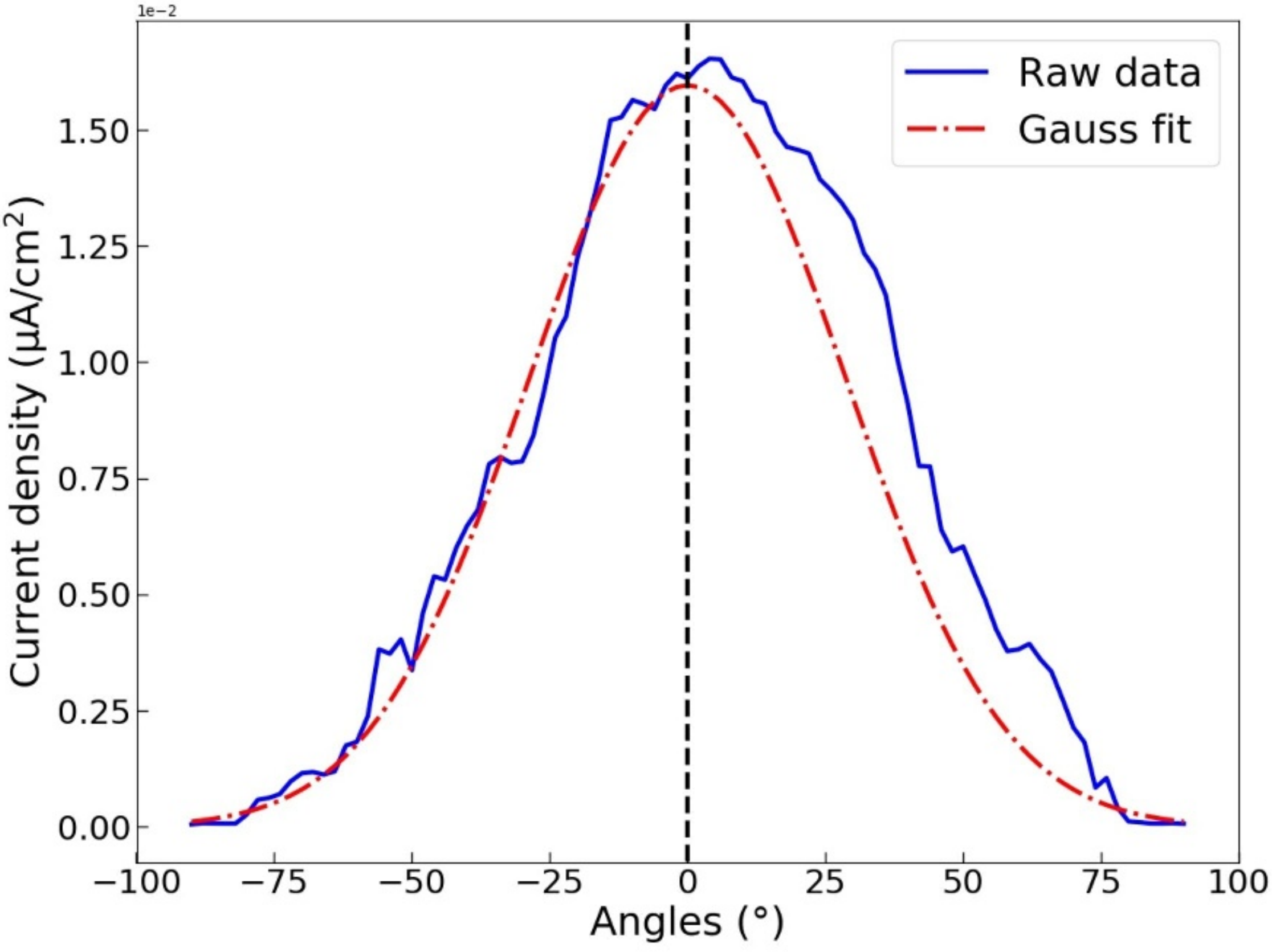
1e−2
Raw data
Gauss fit
Current density (μA/cm²)
1.50
1.25
1.00
0.75
0.50
0.25
0.00
−100
−75
−50
−25
0
25
50
75
100
Angles (°)

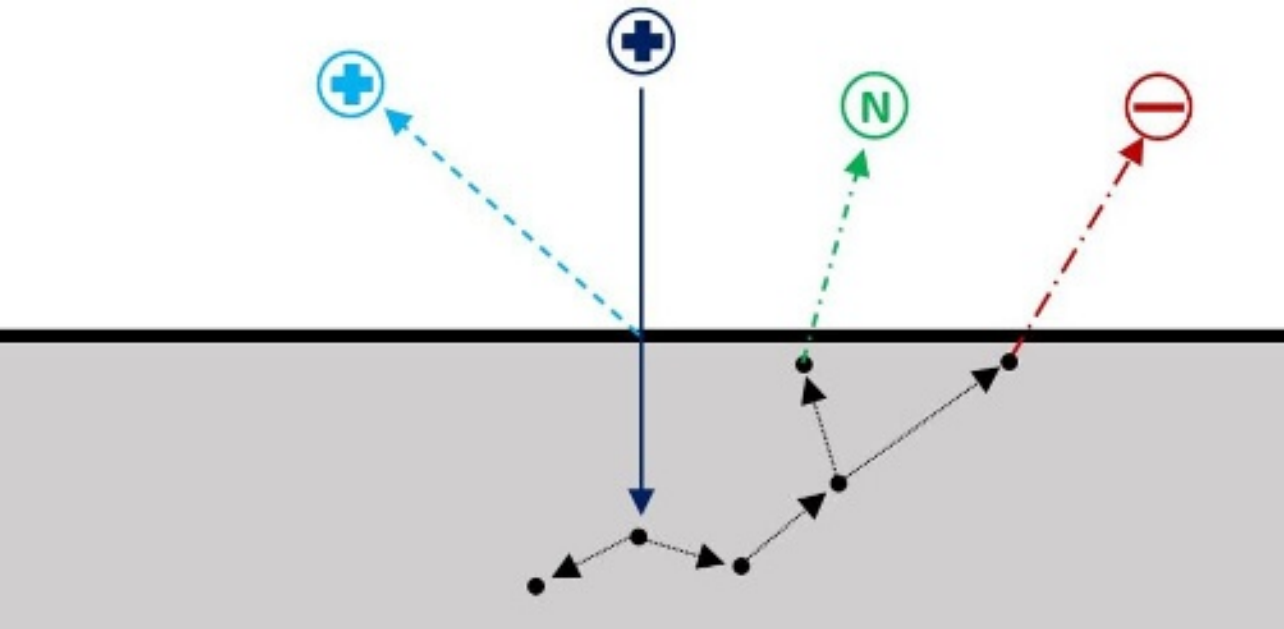
N

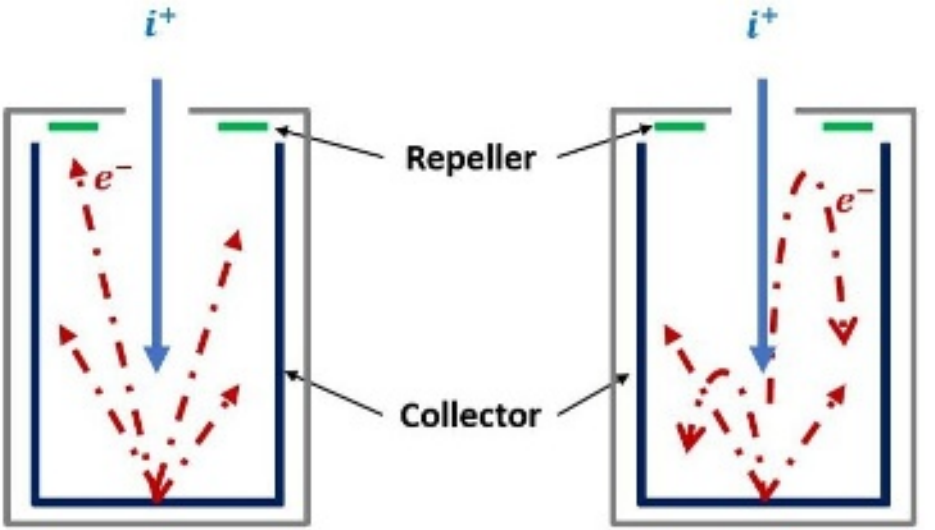

Case 1

$V_c < V_r \leq 0$

$I_c = I_{i_{meas}} + \gamma_{L_{SE}} I_{i_{meas}}$

Case 2

$V_r < V_c < 0$

$I_c = I_{i_{meas}}$

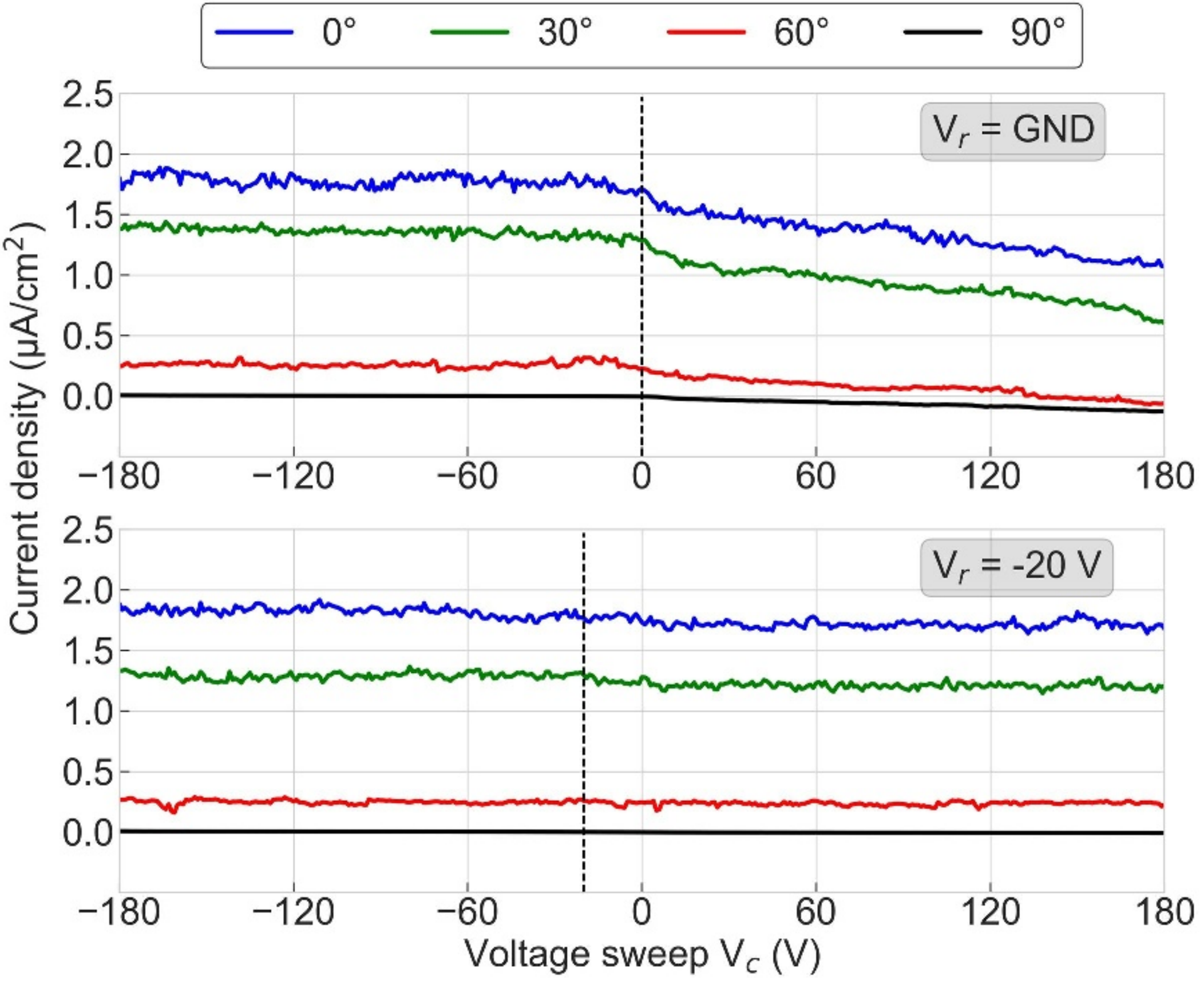
0°
30°
60°
90°
V_r = GND
V_r = -20 V
Current density (μA/cm^2)
Voltage sweep V_c (V)
2.5
2.0
1.5
1.0
0.5
0.0
−180
−120
−60
0
60
120
180

Zone 1

$V_c < V_r < 0$

Zone 2

$V_r < V_c < 0$

Zone 3

$V_r < 0 < V_c$

Collector current

Repeller current

V_r

V_r

Current (μA)

4.00
3.75
3.50
3.25

0.15
0.10
0.05

−150 −100 −50 0 50 100 150

Collector voltage V_c (V)

50 mm
30 mm
10 mm

$V_{repeller}$ = -20 V

$V_{collector} < V_{repeller}$

$V_{collector} > V_{repeller}$

Collector current (μA)

1.8
1.6
1.4
1.2
1.0
0.8
0.6
0.4
0.2
0.0

−150
−100
−50
0
50
100
150

Collector voltage sweep

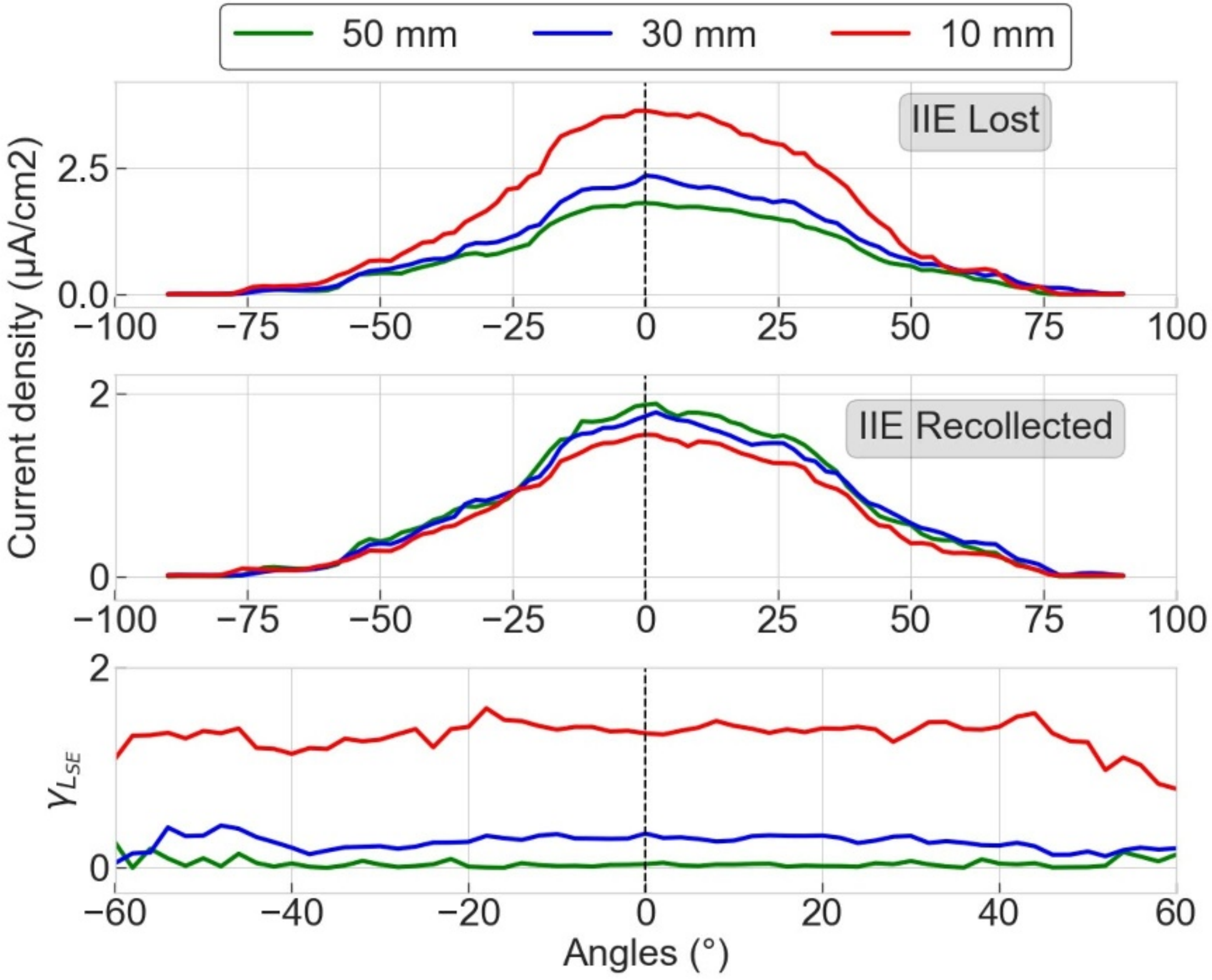
50 mm
30 mm
10 mm
IIE Lost
IIE Recollected
Current density (μA/cm2)
2.5
0.0
2
0
−100
−75
−50
−25
0
25
50
75
100
$\gamma_{L_{SE}}$
−60
−40
−20
20
40
60
Angles (°)

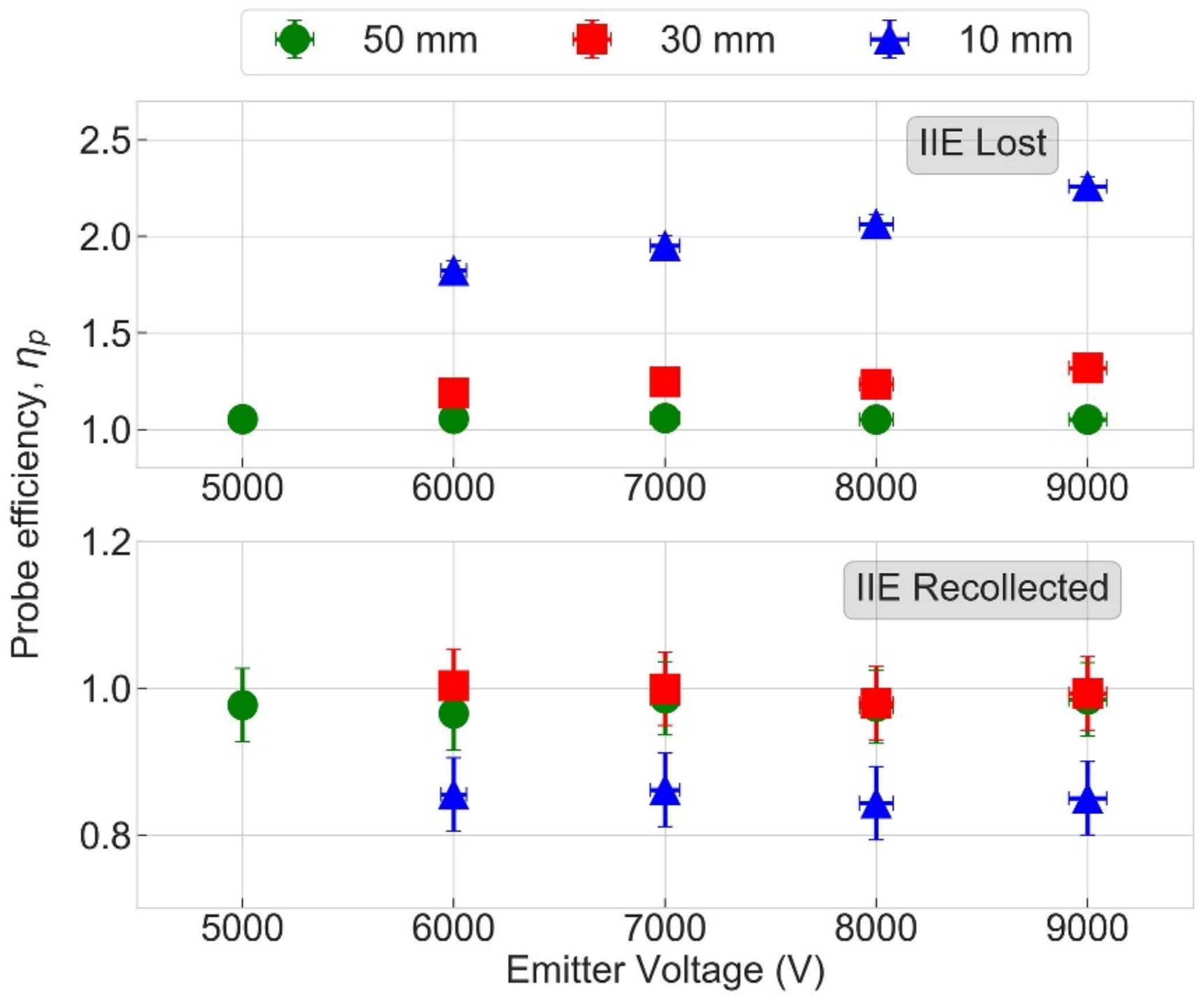
50 mm
30 mm
10 mm
IIE Lost
IIE Recollected
Probe efficiency, η_p
Emitter Voltage (V)
2.5
2.0
1.5
1.0
1.2
0.8
5000
6000
7000
8000
9000

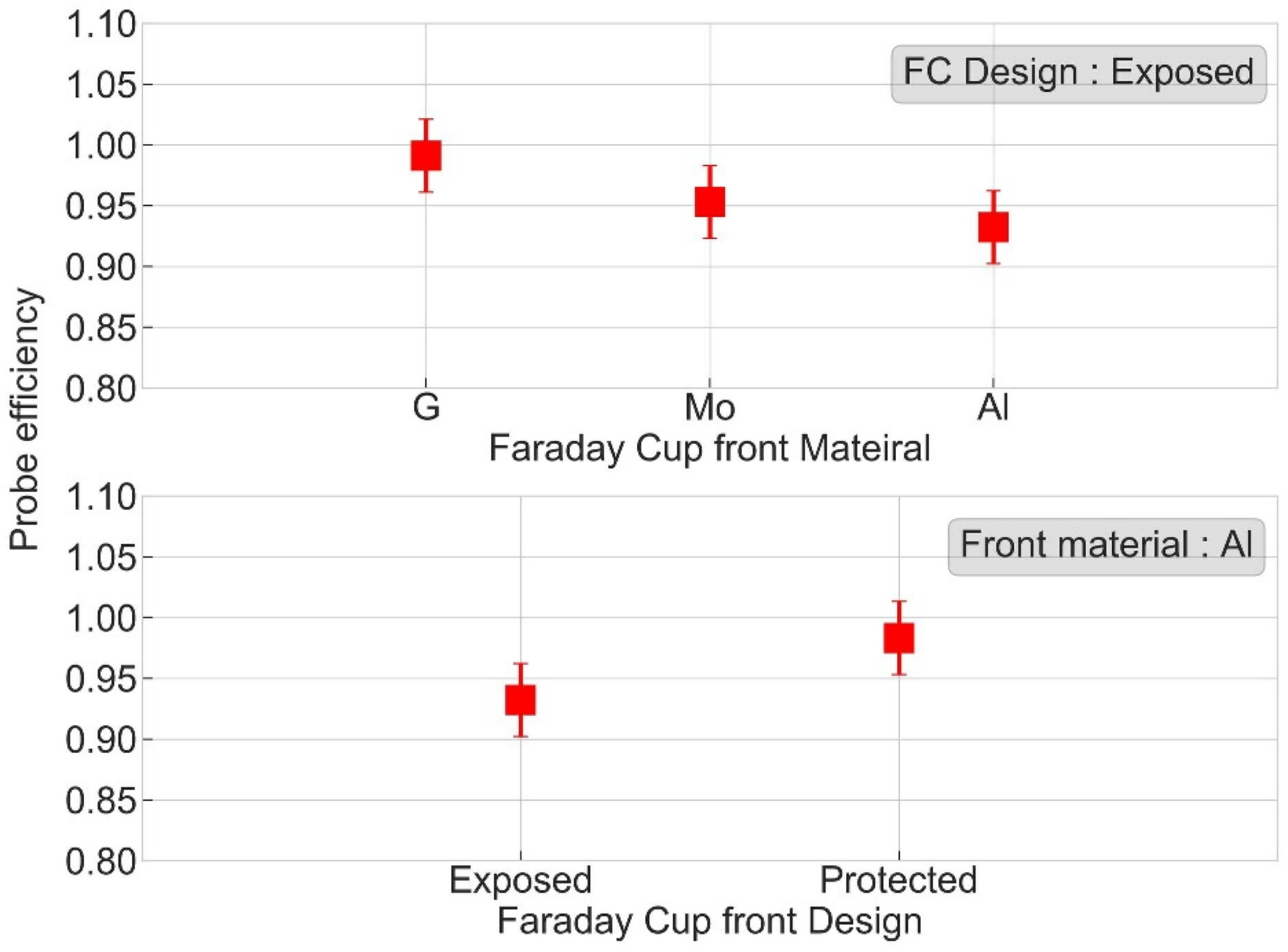
Probe efficiency
1.10
1.05
1.00
0.95
0.90
0.85
0.80
FC Design : Exposed
G
Mo
Al
Faraday Cup front Mateiral
Front material : Al
Exposed
Protected
Faraday Cup front Design

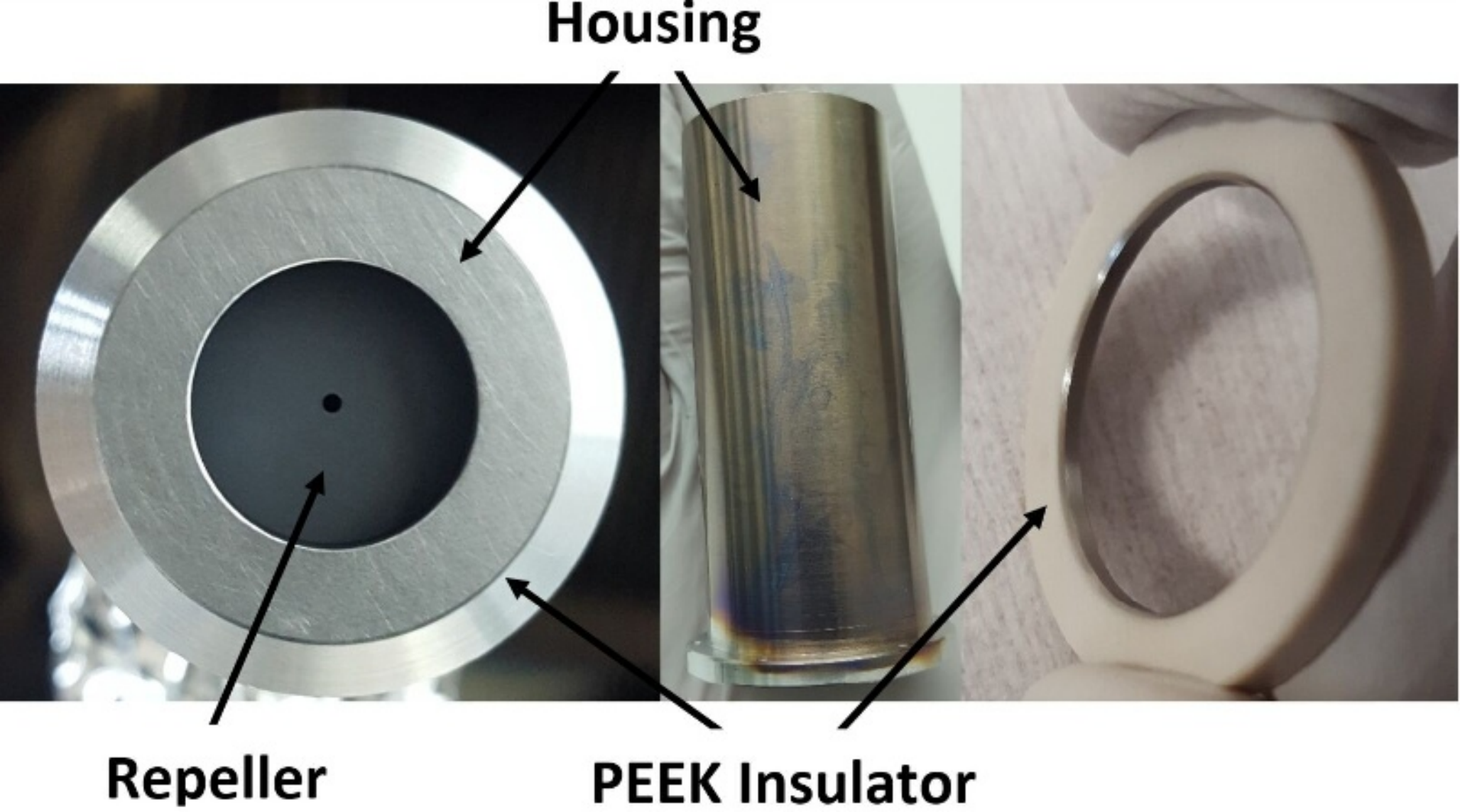
Housing
Repeller
PEEK Insulator

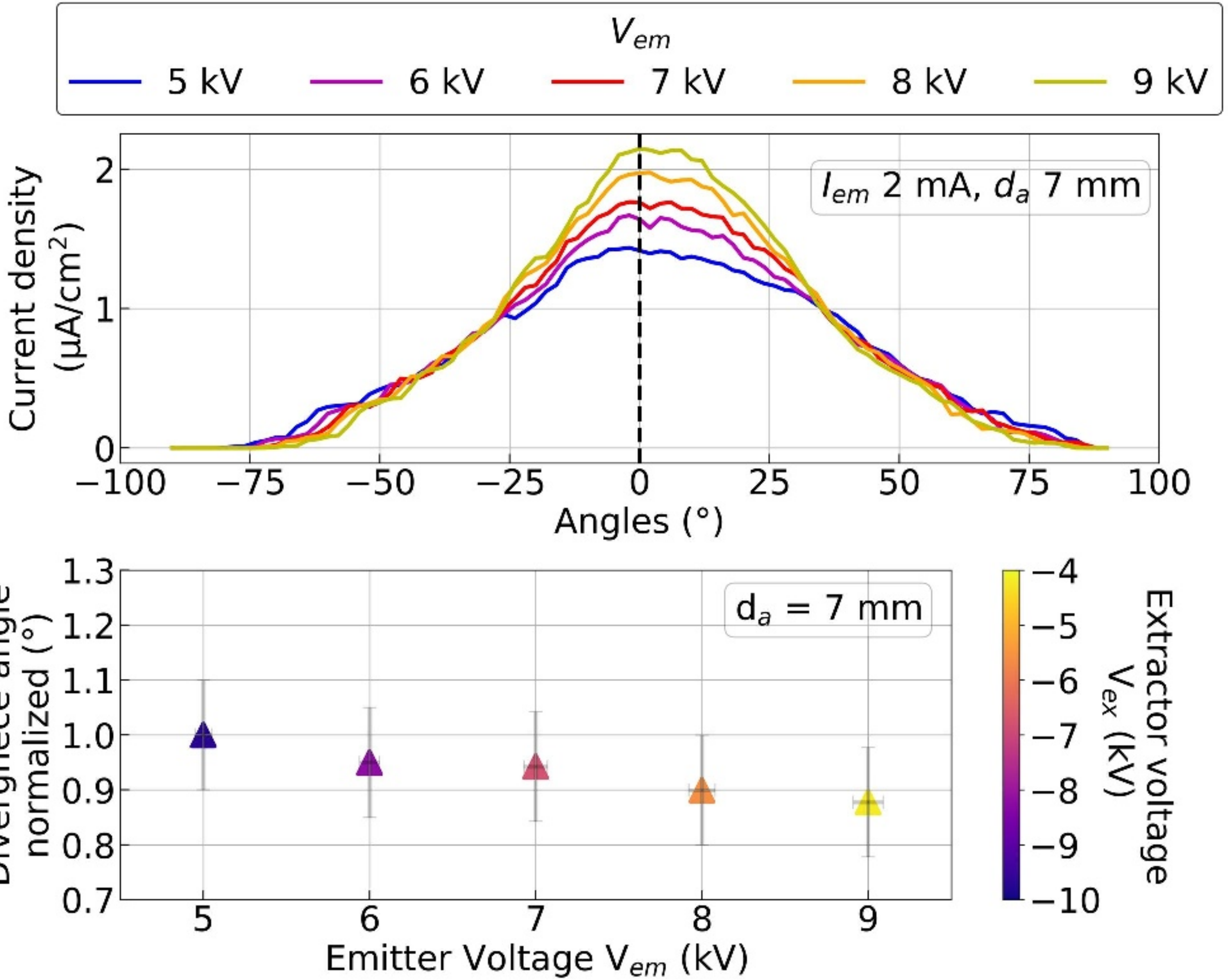
V_{em}
5 kV
6 kV
7 kV
8 kV
9 kV
I_{em} 2 mA, d_a 7 mm
Current density (μA/cm²)
2
1
0
−100
−75
−50
−25
0
25
50
75
100
Angles (°)
d$_a$ = 7 mm
Divergnece angle normalized (°)
1.3
1.2
1.1
1.0
0.9
0.8
0.7
5
6
7
8
9
Emitter Voltage V$_{em}$ (kV)
−4
−5
−6
−7
−8
−9
−10
Extractor voltage V$_{ex}$ (kV)

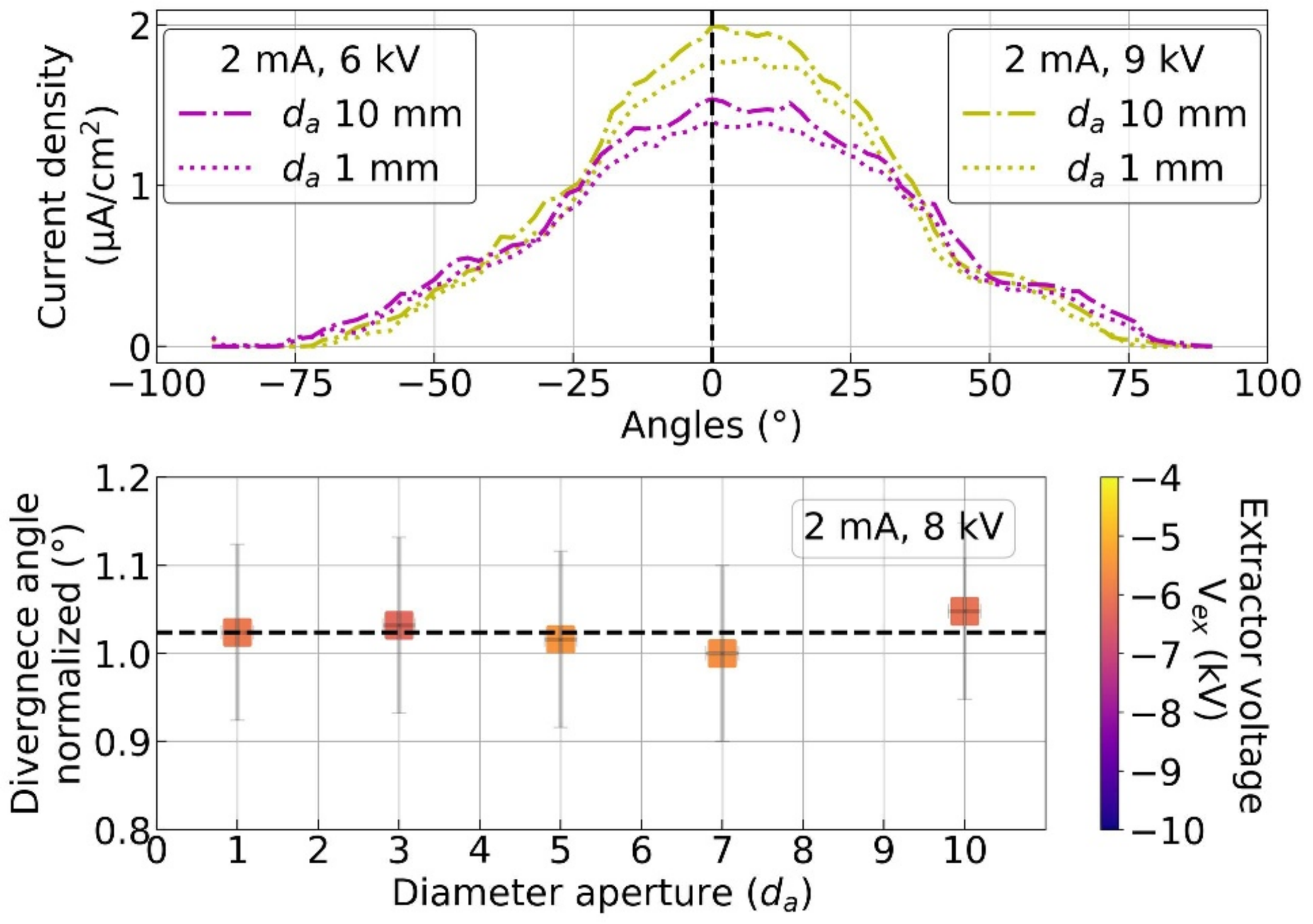
2 mA, 6 kV
d_a 10 mm
d_a 1 mm
2 mA, 9 kV
d_a 10 mm
d_a 1 mm
Current density (μA/cm²)
Angles (°)
2 mA, 8 kV
Divergnece angle normalized (°)
Diameter aperture (d_a)
Extractor voltage V_{ex} (kV)

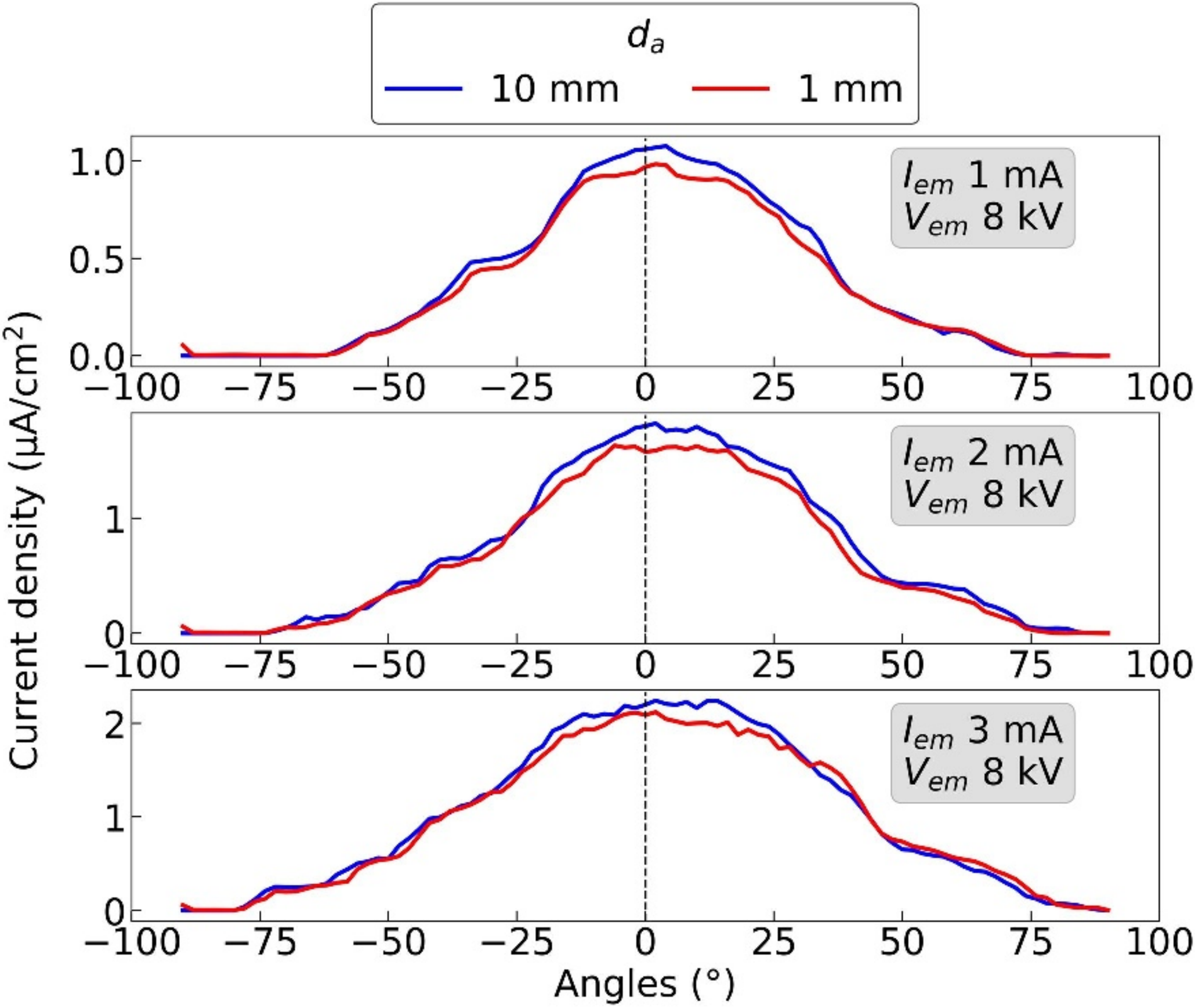
d_a
10 mm
1 mm
I_{em} 1 mA
V_{em} 8 kV
I_{em} 2 mA
V_{em} 8 kV
I_{em} 3 mA
V_{em} 8 kV
Current density (μA/cm^2)
Angles (°)

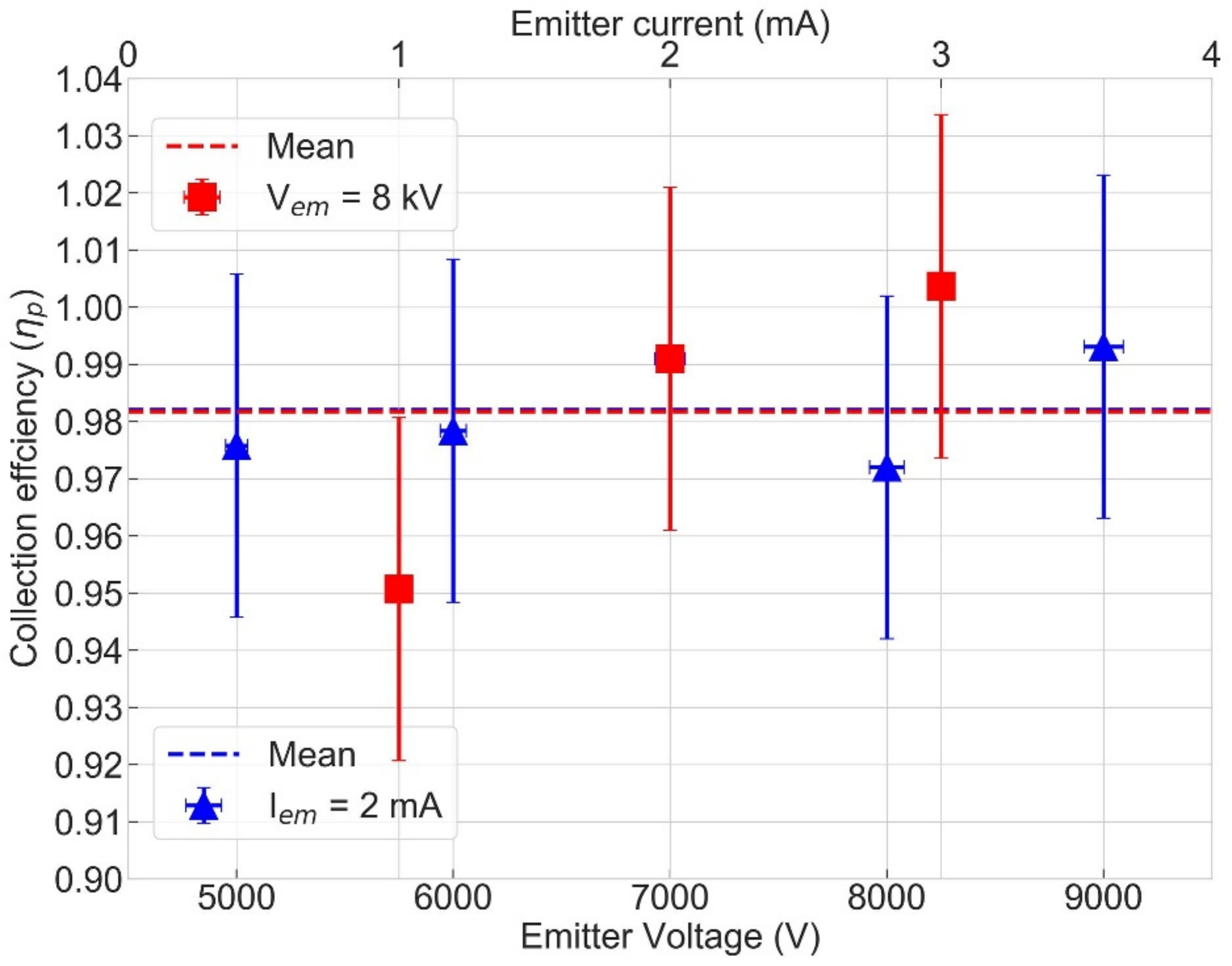
Emitter current (mA)
0
1
2
3
4
1.04
1.03
1.02
1.01
1.00
0.99
0.98
0.97
0.96
0.95
0.94
0.93
0.92
0.91
0.90
Collection efficiency (η_p)
Mean
V_{em} = 8 kV
Mean
I_{em} = 2 mA
5000
6000
7000
8000
9000
Emitter Voltage (V)

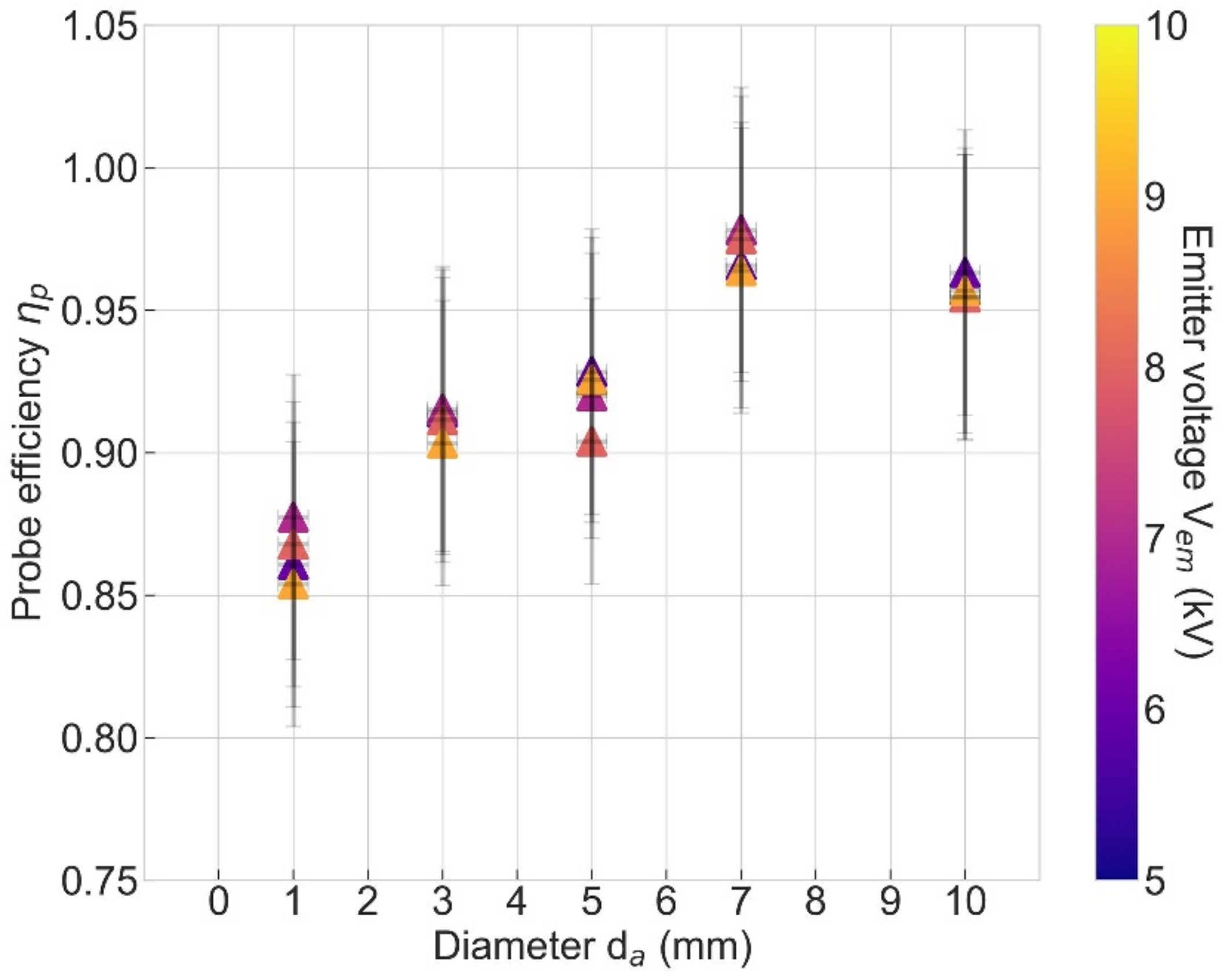
1.05
1.00
0.95
0.90
0.85
0.80
0.75
Probe efficiency η_p
0
1
2
3
4
5
6
7
8
9
10
Diameter d_a (mm)
10
9
8
7
6
5
Emitter voltage V_{em} (kV)

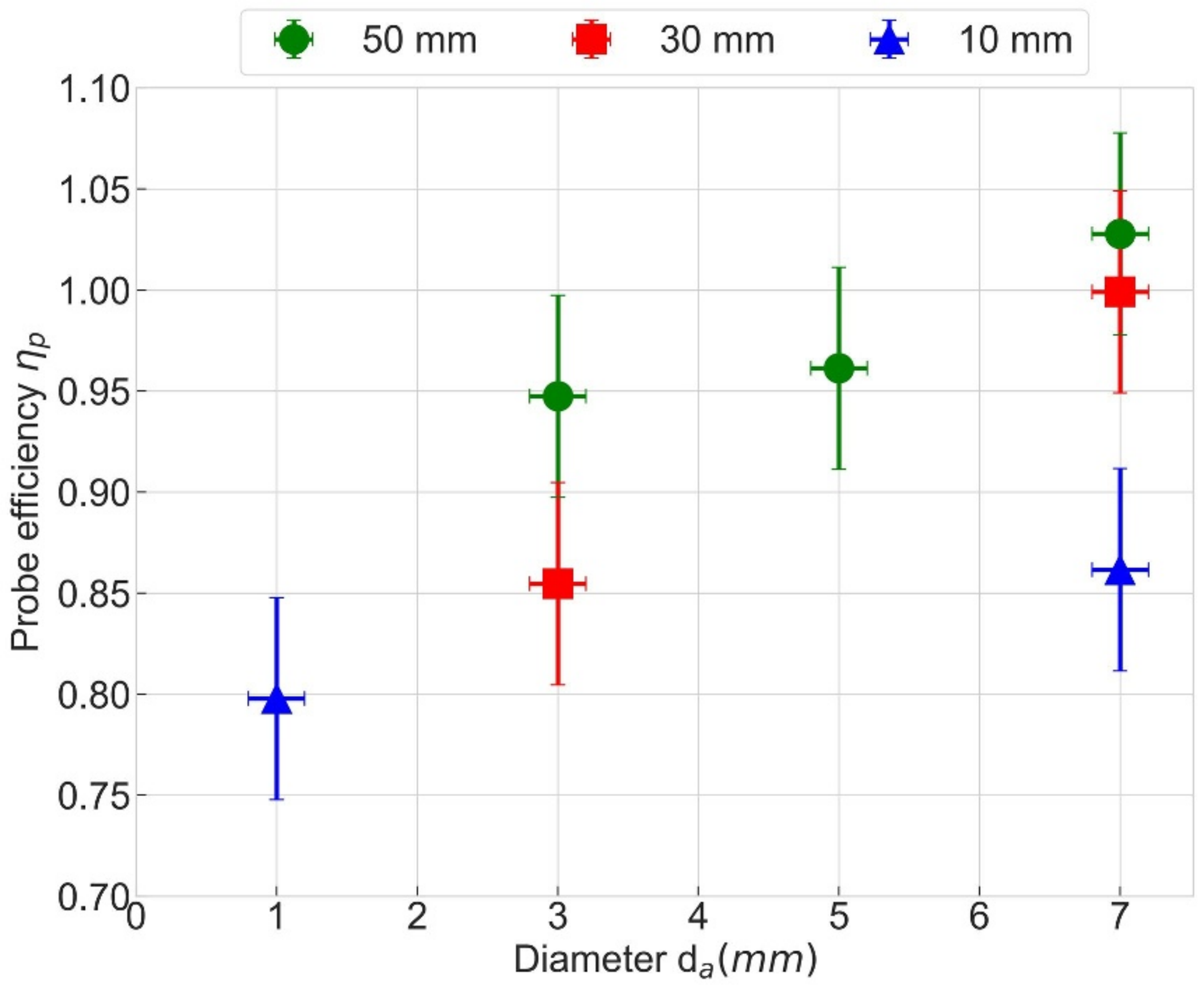
50 mm
30 mm
10 mm
1.10
1.05
1.00
0.95
0.90
0.85
0.80
0.75
0.70
Probe efficiency η_p
0
1
2
3
4
5
6
7
Diameter $d_a(mm)$

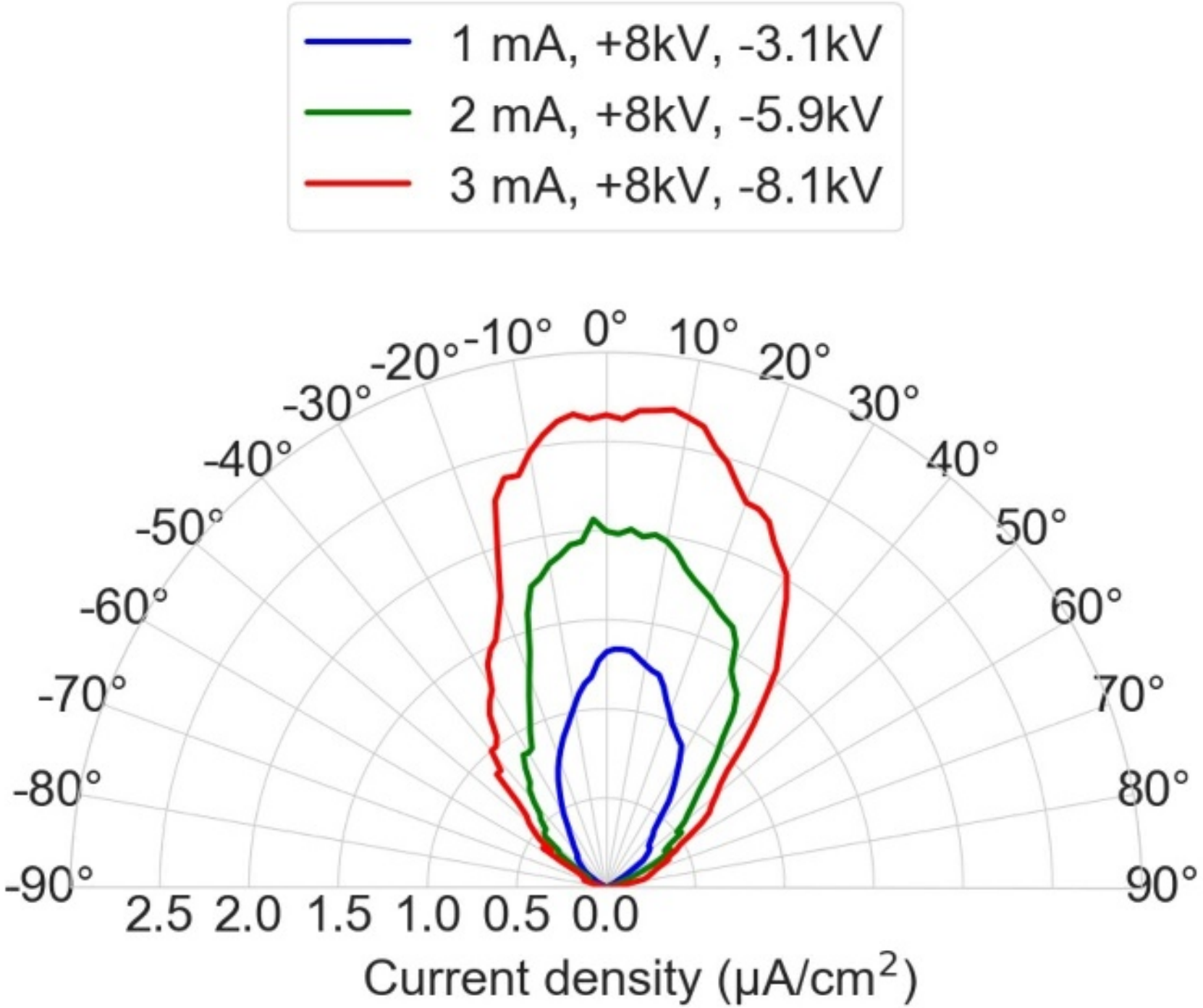
1 mA, +8kV, -3.1kV
2 mA, +8kV, -5.9kV
3 mA, +8kV, -8.1kV
0°
10°
20°
30°
40°
50°
60°
70°
80°
90°
-10°
-20°
-30°
-40°
-50°
-60°
-70°
-80°
-90°
2.5 2.0 1.5 1.0 0.5 0.0
Current density (μA/cm²)

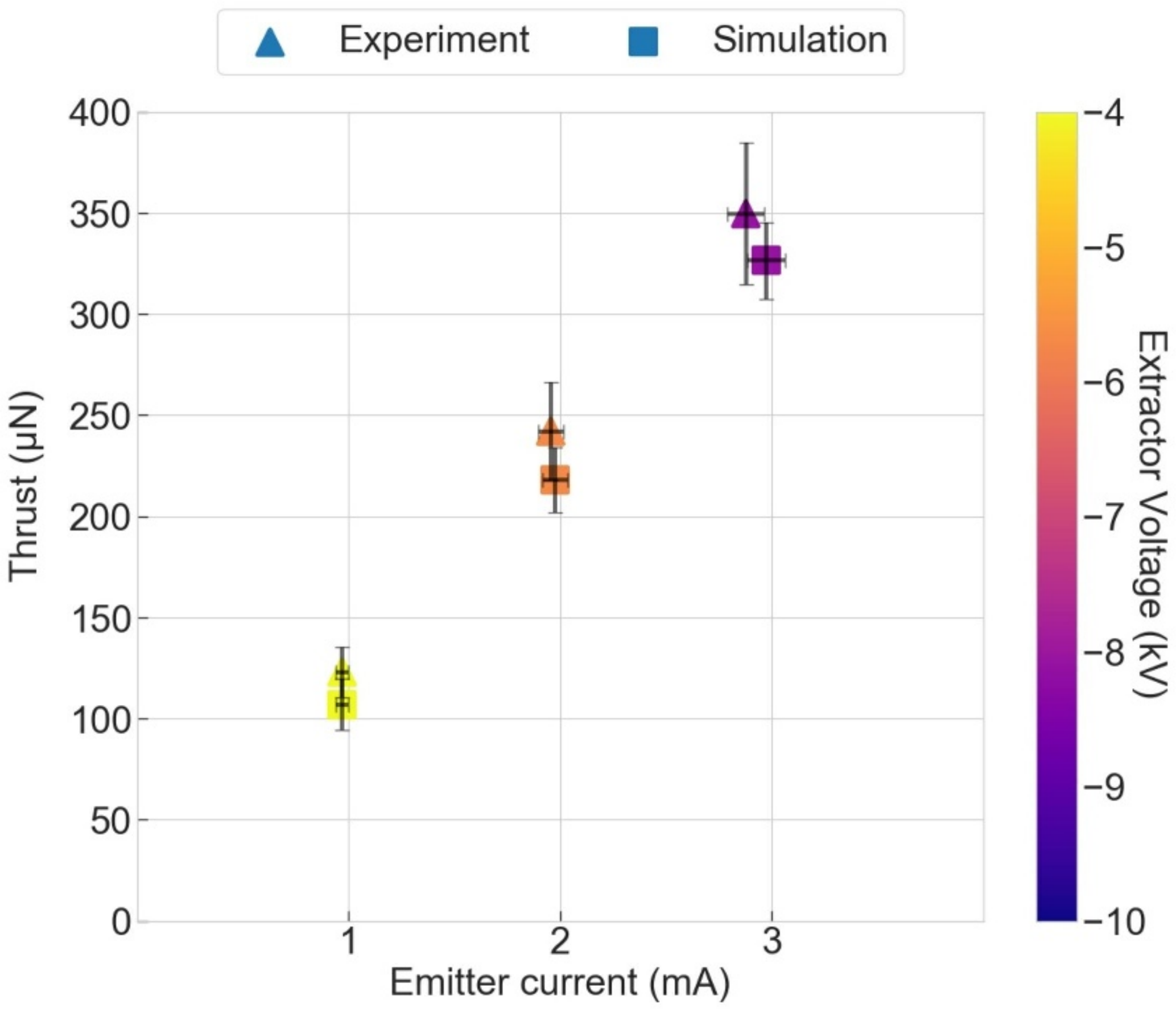
Experiment
Simulation
Thrust (μN)
400
350
300
250
200
150
100
50
0
1
2
3
Emitter current (mA)
Extractor Voltage (kV)
−4
−5
−6
−7
−8
−9
−10